

An Experimental Comparison of Transfer Learning against Self-supervised Learning

Zehui Zhao^{a,b}, Laith Alzubaidi^{b,c,*}, Jinglan Zhang^{a,b}, Ye Duan^d, Usman Naseem^e and Yuantong Gu^c

^aSchool of Computer Science, Queensland University of Technology, Brisbane, 4000, QLD, Australia

^bCentre for Data Science, Queensland University of Technology, Brisbane, 4000, QLD, Australia

^cSchool of Mechanical, Medical, and Process Engineering, Queensland University of Technology, Brisbane, 4000, QLD, Australia

^dSchool of Computing, Clemson University, Clemson, 29631, SC, USA

^eSchool of Computing, Macquarie University, Sydney, 2109, NSW, Australia

ARTICLE INFO

Keywords:

Transfer learning
Self-supervised learning
Double fine-tuning
Imbalanced datasets
XAI
Medical images

ABSTRACT

Recently, transfer learning and self-supervised learning have gained significant attention within the medical field due to their ability to mitigate the challenges posed by limited data availability, improve model generalisation, and reduce computational expenses. Leveraging pre-trained features from analogous domains, these methodologies prove instrumental in improving model performance and addressing data scarcity issues stemming from the privacy concerns associated with patient data sharing and the exorbitant costs involved in collecting medical test data. Consequently, transfer learning and self-supervised learning hold immense potential for advancing medical research. However, it is crucial to recognise that transfer learning and self-supervised learning architectures exhibit distinct advantages and limitations, manifesting variations in accuracy, training speed, and robustness. Asserting the superiority of one method over the other across all contexts is irresponsible, leaving researchers grappling with the challenge of selecting the most fitting method and configuration for their specific scenarios. This not only engenders confusion during method selection, but also leads to inefficient utilisation of computational resources, potentially compromising the reliability of experimental outcomes. To address this dilemma, we carried out a comparative study between transfer learning and self-supervised learning methods through experimentation. Two widely adopted deep learning models, Xception and ResNet, were employed to extract features under transfer learning and self-supervised learning settings respectively. Subsequently, these pre-trained models underwent fine-tuning and testing using both colourful (Kvasirv2, EyePacs) and grey-scale (BusI, chest CT) medical datasets. The findings of this study revealed that transfer learning setting demonstrated better performance on colourful datasets, achieving an accuracy of 96.4% on the Kvasirv2 dataset and 92.1% on the EyePacs dataset. In contrast, the self-supervised learning method has shown superior performance on grey-scale datasets, achieving an accuracy of 90% and 97.22% on BusI and chest CT datasets, both exceeding recent state-of-the-art models. Furthermore, considering the data imbalance problem and domain mismatch issue that occurs frequently in the medical field, we conducted experiments using two data-altering techniques (data augmentation and down-sampling) and the double fine-tuning technique combined with proposed pre-trained transfer learning and self-supervised learning models to compare their efficiency in handling those issues. The experimental result reveals that the data augmentation method can improve the robustness of pre-trained models towards imbalanced data, while the down-sampling methods have minor improvements. The double fine-tuning technique has been proved to effectively reduce the domain mismatch problem without using a large number of pre-training data. This comprehensive analysis investigates the influence of colour information, dataset size, and dissimilar transfer issues in the medical field, and uses explainable artificial intelligence techniques to evaluate the reliability of the pre-trained models. The insights gleaned from this research provide valuable guidance in selecting the appropriate pre-training settings in various scenarios, with potential applications extending beyond medical research.

1. Introduction

Transfer Learning (TL) and Self-supervised Learning (SSL) methodologies strive to enhance the performance of Convolutional Neural Networks (CNNs) in target domains by capitalising on preexisting knowledge derived from analogous domains. In recent years, these techniques have emerged as pivotal contributors to advances in computer

vision, particularly within the medical domain. Their significance lies in mitigating data dependence during the training of high-performance deep learning (DL) models, while simultaneously reducing computational costs and training time. Traditional supervised DL architectures, exemplified by models such as AlexNet (Krizhevsky et al., 2012) and ResNet (He et al., 2016), are based heavily on abundant, well-labelled data for feature acquisition and subsequent task support. In the medical realm, where data annotation requires expert intervention, the scarcity and expense of labelled data make the architectures employing TL and SSL methods increasingly appealing. These methods not only elevate model performance and alleviate overfitting risks,

*Corresponding author

Email addresses: zehui.zhao@hdr.qut.edu.au (Z. Zhao),

l.alzubaidi@qut.edu.au (L. Alzubaidi), jinglan.zhang@qut.edu.au (J. Zhang), duan@clemson.edu (Y. Duan), usman.naseem@mq.edu.au (U. Naseem), yuantong.gu@qut.edu.au (Y. Gu)

but also enhance model reusability. The success of pre-trained methods is largely due to the advent of ImageNet (Russakovsky et al., 2015), a massive publicly available dataset comprising more than 1.2 million images classified into 1,000 classes. ImageNet's rich data repertoire facilitates seamless knowledge transfer to diverse fields, notably contributing to the effectiveness of pre-trained models.

In the medical domain, transfer learning has undergone extensive refinement, producing various designs and improvements that increase its efficacy in various diseases (Niu et al., 2020). In contrast, self-supervised learning, a more recent entrant, has gained prominence by achieving state-of-the-art supervised representation learning model performance without relying on additional manual annotations. Recognising the practical importance of TL and SSL in computer vision tasks, researchers have diligently benchmarked their performance, seeking information for future architectural advancements (Hosseinzadeh Taher et al., 2021). Recent investigations encompass diverse aspects such as the suitability of different architectures, the relevance of source and target domains, the exploration of various pretext tasks, analysis of the impact of the size of the pre-training dataset, and evaluation of the model capacity on the performance of downstream tasks (Neyshabur et al., 2020; Ericsson et al., 2022b). Despite the strides made in TL and SSL studies, emerging research suggests that the ubiquitous ImageNet may not be optimal for the medical field (Raghu et al., 2019). The inherent dissimilarity between natural images in ImageNet and medical images raises concerns about domain mismatch adversely affecting downstream task training. A 'medical version ImageNet' is conspicuously absent, compelling researchers to turn to SSL methods that do not need manual labels during pre-training. However, there is still a notable gap in understanding how well these pre-training methods perform in various scenarios.

Based on our recent study (Zhao et al., 2023), we observed that the majority of recent TL methods still tend to operate within a supervised learning framework, allowing models to acquire features from meticulously annotated data. In contrast, SSL methods are performed under the unsupervised learning setting by leveraging data augmentation techniques to create corresponding pseudo-labels, eliminating the necessity for conventional human supervision during training. This methodological contrast yields distinctive strengths and weaknesses in data types, sizes, and domains. However, the limited understanding of these two pre-trained methods has resulted in adverse effects on model performance and robustness across varied environments. This gap places an increased burden on researchers, necessitating a nuanced understanding of both methods and amplifying time and computational costs in numerous research endeavours.

Some researchers have begun to take note of this knowledge gap between TL and SSL methods and have endeavoured to address this issue. Yang et al. (2020) have conducted a comparative experiment of the two pre-training methods to analyse the impact of domain similarity on the two pre-training methods, across various source and target

domains, covering daily objects, natural environments, and even medical data. However, their research did not consider the difference and influence of image colour information, target dataset size, and data imbalance issues, which are important conditions in the training process and have often faced challenges in the medical field. Moreover, they did not consider the robustness of their model, since it is vital for models to provide explainable and reliable answers instead of simply providing the correct answers in the medical field. Azizi et al. (2023) elucidated the benefits of the SSL method, noting its ability to achieve comparable performance with TL models while using less than 10% of the target domain data. However, their investigation primarily focused on the development of sophisticated SSL architectures rather than undertaking a comprehensive comparative analysis of the two methodologies.

To solve the current knowledge gap between TL and SSL methods and provide supporting evidence to our previous work, this study aims to dive deeper into the factors that influence the performance of TL and SSL methods and provide guidance to researchers in choosing suitable pre-training settings. A comparative experiment using both pre-trained methods was designed to identify the effectiveness of these pre-training methods in multiple imaging modalities and recognising potential limitations is of utmost importance. Meanwhile, we utilised two data-altering methods including data augmentation and down-sampling to solve the data imbalance problem that occurred in the target datasets and employed the double fine-tuning technique to solve the potential domain mismatch issues between source data and target medical data. Furthermore, one Explainable Artificial Intelligence (XAI) technique was used to analyse the reliability and robustness of two pre-trained models, providing evidence for the pre-trained models in learning useful features. The knowledge gained from this study will streamline the experimental setup phase, saving valuable time and resources, and pave the way for future advancements in both the TL and SSL methods. Thus, we would like to emphasise the contributions of this study to knowledge:

1. To the best of our knowledge, this is the first comparative evaluation between TL and SSL methods that compare their strengths and weaknesses on different colourful and grey-scale medical datasets.
2. A detailed review of the pre-trained TL and SSL methods across varied target dataset sizes revealed nuanced performance dynamics, demonstrating better stability of the pre-trained SSL method towards small datasets compared to the TL method.
3. The XAI technique has been used in analysing the two pre-trained methods, elucidating the superior reliability and robustness of the SSL method compared to the TL method.
4. An examination of two data-altering techniques coupled with pre-trained methodologies has been conducted to address data imbalance issues, elucidate the pronounced effectiveness and performance superiority of the data-augmentation technique.

5. A strategic application and evaluation of the double fine-tuning technique within the proposed pre-trained models underscored its instrumental role in augmenting the models' performance and fortifying their robustness.

6. The proposition of two pre-trained models, instantiated using TL and SSL methods, produced results that exceeded current state-of-the-art CNN models on various publicly available medical datasets.

This introduction section provides background and contributions of our research; the subsequent segments of the paper are organised as follows: The second section delves into the current applications and research of DL, TL, and SSL methods in the medical field and reveals several common limitations within pre-trained methods. The third section then presents the details of the datasets used and outlines the methods proposed in this study, elucidating the experimental process. The fourth section compiles the results of the experiment and performs a comparative analysis of the performance of the two pre-trained methods, demonstrating their effectiveness in diverse medical datasets. Finally, the last section summarised the findings of this study, providing a guideline for selecting appropriate pre-trained methods in various medical application scenarios.

2. Literature Review

In this section, we briefly review the applications of deep learning, transfer learning, and self-supervised learning in the field of medical imaging. Additionally, we highlight recent constraints encountered in the application of transfer learning and self-supervised learning within medical contexts.

2.1. Deep Learning for Medical Imaging Tasks

Deep learning has emerged as a highly promising technique for various analytical tasks, encompassing classification, segmentation, and generation. Within the medical field, the primary objective of DL models is to detect and locate diseases quickly and efficiently, assisting physicians in rapid diagnoses. As these models demonstrate considerable prowess in medical tasks, an increasing number of DL models are proposed and implemented in this domain. However, the performance of DL models in medical imaging tasks is fundamentally dependent on the volume of the dataset, and data scarcity remains a persistent challenge in the medical field (Wang, 2021). This limitation comes from various reasons, such as privacy concerns, that prevent medical agencies from disseminating patient records, which is the most prevalent (Razzak et al., 2018). In addition, financial costs and the need for professional knowledge to collect high-quality medical data with annotations contribute to this scarcity. Consequently, data scarcity in the medical field has limited the development of DL, and researchers have devised technical solutions, such as data augmentation and pre-trained methods like TL or SSL, to address this issue.

2.2. Transfer Learning for Medical Imaging Tasks

Transfer learning, also known as knowledge transfer, is a machine learning (ML) technique that utilises the knowledge acquired from one task to improve performance on a related task. The objective of the TL method is to enrich the learnt feature of the pre-trained model and reduce its data dependence (Pan & Yang, 2010). With the proliferation of deep learning, transfer learning has become integral to various applications, particularly in the medical field. Numerous studies have explored the factors that contribute to the success of transfer learning in CNNs. These factors include choosing an optimal deep learning architecture for guaranteed model performance (Kornblith et al., 2019), choosing source domains that share a close distribution to the target domain to accelerate better transfer performance (Zhang et al., 2022), and increasing the size of the source datasets and pre-trained model parameters for richer knowledge transfer (Kolesnikov et al., 2020). In particular, a central drawback of TL pre-training is the requirement for a large quantity of costly manually supervised training (Huh et al., 2016), which requires a substantial pretext dataset such as ImageNet for successful pre-trained learning. To address this issue, researchers also designed fully unsupervised TL architectures to avoid requiring additional labels, but the performance has turned out to be too weak. The prevailing standard in transfer learning architectures in medical imaging involves utilising ImageNet as a source domain and fine-tuning it with medical-related target datasets. Despite the positive results reported with pre-trained ImageNet models on colourful target datasets (Morid et al., 2021; Patil & Sharma, 2024), questions have arisen regarding the suitability of ImageNet for the grey-scale medical datasets (Raghu et al., 2019). Evidence suggests that the transfer learning method does not consistently produce favourable results in the medical domain (Alzubaidi et al., 2020), as ImageNet representations do not align well with those of medical images, particularly grey-scale ones.

2.3. Self-supervised Learning for Medical Imaging Tasks

Self-supervised learning is a recently appeared unsupervised pre-training method that employs model-augmented data as pseudo-labels to provide supervision signals during the pre-training process. Compared to the transfer learning method, self-supervised learning appears particularly attractive in the medical field, offering an effective solution to use large amounts of unlabelled data (Shurrah & Duwairi, 2022). Notably, the self-supervised learning model exhibits improved accuracy performance by incorporating more complex auxiliary tasks and leveraging model-generated pseudo-labels to facilitate the learning of powerful features from unlabelled data. Some studies have indicated that self-supervised learning models, particularly those employing contrastive methods, tend to learn invariant features by maximising similarities between raw input data and self-generated pseudo labels (Ericsson et al., 2022a). This suggests that contrastive self-supervised learning methods are inclined to overlook changeable feature information,

Table 1
Limitations of recent pre-trained methods in the medical field.

Author	Methods	Descriptions
Del Pup & Atzori (2023)	Self-Supervised Learning	SSL lacks comparison with supervised learning methods when the amount of supervision that can be provided for the downstream task is sufficiently high.
Wu et al. (2023)	Self-Supervised Learning	Some transfer learning studies just treated SSL pre-training method as an alternative scheme to improve the performance of downstream tasks.
Zhao et al. (2023)	TL & SSL	Lacks specific experiments in comparison of TL and SSL methods' performance, generalisability, and robustness.
Limitation: Lacks systematic comparison between pre-trained methods		
Romero et al. (2020)	Transfer Learning	Pre-trained TL model with ImageNet weight does not bring advantages to X-ray based classification tasks.
Alzubaidi et al. (2021)	Transfer Learning	Pre-trained features from ImageNet mismatch medical images.
Atasever et al. (2023)	Transfer Learning	Transferring information obtained from natural images are less successful than lighter methods trained from scratch.
Tan et al. (2024)	Self-Supervised Learning	Significant differences exist between COVID-19 medical images and pre-trained natural samples, and need more information to guide the reconstruction of target images.
Limitation: Domain discrepancy		
Muljo et al. (2023)	Transfer Learning	Pre-trained TL model only have limited positive impacts when facing an imbalanced medical dataset.
Zhang et al. (2023)	Self-Supervised Learning	Data bias in both pre-training and target data affects representation learning, leading to poor target performance.
Limitation: Imbalanced datasets		
Qayyum et al. (2020)	Transfer Learning	The learning process of models is complex and fails to provide the knowledge needed. explanations for learning behaviour and prediction-making process.
Schiappa et al. (2023)	Self-Supervised Learning	The lack of explainability has prevented the understanding of pretext and downstream task learning process, and constrained further improvement of the SSL model.
Limitation: Lack of additional interpretability		

resulting in increased stability when confronted with disease images that have unaltered features. Despite certain self-supervised learning studies that have utilised ImageNet with self-supervised pre-training methods for medical imaging tasks and achieved positive results (Truong et al., 2021), there remains a lack of conclusive evidence to ascertain whether pre-trained models with self-supervised learning methods can consistently outperform transfer learning methods in medical imaging tasks and potentially become a new standard in this domain.

2.4. Recent Limitations of Transfer Learning and Self-supervised Learning for Medical Imaging Tasks

The success of the TL and SSL methods in the medical domain is undeniable; however, several challenges impede their further advancement and the full realisation of their potential. Table 1 encapsulates some of these limitations, and our study aims to dissect and address these challenges, offering insights to guide future researchers in leveraging pre-trained methods effectively.

In summary, four overarching limitations hinder the progress of pre-trained models. These encompass the lack of comprehension and comparison between pre-trained methods, risks associated with domain discrepancy and imbalanced datasets, and the dearth of interpretability of the model. Specifically, the limited understanding and comparability between pre-trained methods stem primarily from their architectural level. Despite the fact that TL and SSL methods are both rooted in DL architectures, there has been a

longstanding tendency to perceive them as interchangeable. This overlooks their divergent performance, generalisability across various data types and sizes, and potential representation nuances. Moreover, the opaque nature of DL approaches compounds the challenge of understanding how models extract salient features and make predictions and is exacerbated by the intricate multi-staged training process inherent in pre-trained methods, while many researchers also fail to realise the importance of interpretability. However, raising the understanding of the model's prediction is particularly pertinent in the medical realm, where diagnostic decisions must be rigorously accountable.

Conversely, domain mismatch and data imbalance issues manifest at the data level. Domain mismatch arises when the representation and distribution of domain data diverge from the target data, which is a common concern in pre-trained methods but exacerbated in medical applications because of the dissimilarity between publicly available pre-training datasets (e.g., ImageNet) and medical contexts. Also, data imbalance poses a significant challenge, especially in medical scenarios where target diseases are infrequent and difficult to accumulate in sample sizes equivalent to normal images. These issues have constrained the quality of the features extracted from the pre-training learning process, further leading to inefficient resource utilisation and limited model performance.

Despite the strides made by pre-trained methods in the medical domain, urgent attention is warranted to surmount

Table 2
Details of Datasets.

Datasets	Image Count	Image Category
Grey-scale Image Datasets		
Source Domain Datasets		
VinDr-CXR Nguyen et al. (2022)	18,000	X-ray
CT Kidney Islam et al. (2022)	12,446	CT
OASIS MRI Marcus et al. (2007)	80,000	MRI
Total number	110,446	Grey-scale
Target Domain Datasets		
BusI Al-Dhabyani et al. (2020)	780	Ultrasound
Lung Cancer CT Hany (2020)	900	CT
Colourful Image Datasets		
Source Domain Datasets		
ODIR-2019	14,400	Ophthalmic
ISIC 2019 Combalia et al. (2019)	25,331	Dermoscopic
Total number	39,731	Colourful
Target Domain Datasets		
Kvasirv2 Pogorelov et al. (2017)	8000	Gastrointestinal tract
EyePacs Kiefer et al. (2023)	6000	Fundus

these challenges and propel their further development, capitalising on their potential to revolutionise medical applications.

3. Materials and Method

3.1. Datasets

This section gives a detailed overview of the source and target data used in this study. As aforementioned, the TL and SSL methods have shown different performances towards colourful and grey-scale datasets. The data utilised in this study were also classified into grey-scale and colourful images based on the number of colour channels they possess and the imaging technique used, aiming to compare the strengths and weaknesses of the two pre-trained methods. Table 2 below lists the size and categories of the datasets. In summary, three grey-scale datasets (VinDr-CXR, OASIS MRI, and CT Kidney) were used to pre-train the corresponding greyscale-related downstream tasks, while two colourful datasets (ODIR and ISIC 2019) were selected for training colourful pretext tasks. In addition to the source domain datasets, we selected several publicly available target datasets from different types of commonly researched diseases to ensure generalisability and convenience comparison with the state-of-the-art models. To be specific, two grey-scale datasets (BusI and Lung cancer CT) and two colourful datasets (KvasirV2 and EyePacs) were chosen as the target datasets to assess the performance of pre-trained TL and SSL models. Notably, only the two target grey-scale datasets here are imbalanced datasets, which have a sample size bias within the class.

3.1.1. Grey-scale Image Dataset

Five grey-scale medical datasets originating from diverse modalities and disease backgrounds fulfil the purpose of pre-training and fine-tuning, with the first three datasets used for pre-training, and the last two datasets serving as target datasets for fine-tuning.

1. VinDr-CXR (Nguyen et al., 2022) is an open dataset comprising 18,000 chest X-ray images meticulously collected

from two major hospitals in Vietnam. Radiologists manually annotated all images, providing 22 local labels delineating abnormalities and 6 global labels indicating suspected diseases. The dataset encompasses diseases such as lung tumours, pneumonia, tuberculosis, and chronic obstructive pulmonary disease.

2. CT Kidney (Islam et al., 2022) is a comprehensive CT dataset designed to facilitate automatic kidney tumour diagnosis. It contains a total of 12,446 CT whole abdomen and urinary images, focusing on three primary renal disease categories: kidney stones, cysts, and tumours. Notably, all classes exhibit a consistent mean colour distribution.

3. OASIS MRI is a widely used, publicly available dataset Marcus et al. (2007) gaining popularity as a resource for in-depth analysis of brain MRI images using deep neural networks. This dataset comprises 80,000 brain MRI images categorized into four distinct classes representing different stages of Alzheimer’s disease, primarily supporting tasks related to Alzheimer’s disease detection.

4. BusI (Al-Dhabyani et al., 2020) is a breast ultrasound image dataset for grey-scale breast cancer detection images. The dataset consists of 780 images that are separated into three categories: Benign, Malignant, and Normal, which comprise 210 malignant images, 437 benign images, and 133 normal images along with 433 masked ground truth images that segment the specific disease areas. In this study, we have excluded all the masked images and focused on those real-world image samples.

5. Lung Cancer CT Dataset (Hany, 2020) is a publicly available dataset collected from the Kaggle website, comprising 1000 grey-scaled CT images belonging to four classes, representing three chest cancer types and a normal type: adenocarcinoma, large cell carcinoma, squamous cell carcinoma, and normal cell. The adenocarcinoma class possess 326 image samples, the large cell carcinoma class holds 163 image samples, the normal class has 159 image samples, and the squamous cell carcinoma class reserved 252 image samples.

3.1.2. Colourful Image Dataset

At the same time, four colourful medical datasets have been chosen to support the comparison experiment, with the initial two datasets serving as pre-training sets and the subsequent two datasets employed as target datasets.

1. ODIR-2019 (Peking University International Competition on Ocular Disease Intelligent Recognition) stands as an extensive ophthalmic database encompassing 14,400 vividly coloured images captured from both the left and right eyes. Accompanied by diagnostic keywords provided by medical professionals, the dataset spans eight distinct classes, effectively characterising various diseases and conditions depicted in the images.

2. The ISIC 2019 dataset (Combalia et al., 2019) originated from the ISIC 2019 challenge and comprises 25,331 vibrant dermoscopic images. This dataset encapsulates eight different diseases, including melanoma, melanocytic nevus, basal cell carcinoma, actinic keratosis, benign keratosis,

Table 3
CNN model training options.

Methods	Function	Value
TL & SSL	Execution environment	GPU
SSL	Pretraining epochs	50
TL & SSL	Retraining epochs	50
TL	Fine-tuning epochs	30
TL & SSL	Batch size	64
TL & SSL	Pretrain& Retrain learning rate	1e-03
TL	Fine-tuning learning rate	1e-05
TL & SSL	Shuffle	True
TL & SSL	Optimiser	Adam
TL & SSL	Learning rate schedule	Step-wise

dermatofibroma, vascular lesion, and squamous cell carcinoma. Each image within the dataset is accompanied by its corresponding label, furnishing ground-truth information for comprehensive analysis and training purposes.

3. KvasirV2 dataset (Pogorelov et al., 2017) is a dataset containing 8000 images from inside the gastrointestinal (GI) tract. The data distribution of this dataset is balanced and can be categorised into 8 classes related to anatomical landmarks and endoscopic polyp removal, listed as 'dyed-lifted-polyps', 'dyed-resection-margins', 'esophagitis', 'normal-cecum', 'normal-pylorus', 'normal-z-line', 'polyps', and 'ulcerative-colitis'. Each class consists of 1000 sample images and all of the images have been annotated and sorted by experienced endoscopists.

4. EyePacs dataset (Kiefer et al., 2023) is a generic glaucoma dataset constituted of 6000 fundus images, splitting into two classes of referable glaucoma (RG) and non-referable glaucoma (NRG). The data samples in each class are balanced and have been resized to 256x256 pixels for quick employment to machine learning algorithms and all the data from training and testing directories have been annotated by experts.

3.2. Proposed Methodology

The objective of this experiment is to compare the effectiveness of TL and SSL methods in the medical field and provide evidence for their strengths and weaknesses. Considering the huge time consumption in pre-training models and the limitation in computational resources, we selected two representative DL models including Xception and ResNet to pre-train with TL and SSL methods and compare their performance, stability, and reliability. The workflow diagram for the pre-training stage is shown in Fig. 3 and the workflow diagram for the downstream stage is presented in Fig. 5. The training options are shown in Table 3.

For the TL setting, we selected the Xception architecture (Chollet, 2017) as our base model, which is a widely used DL architecture known for its high performance in various tasks. The Xception module is constructed as a series of three flow structures, each incorporating batch normalisation (BN), rectified linear units (ReLU) activation functions, and separable convolutional kernels in depth. Each module in the Xception model operates through sequential processing:

first through the entry flow, then via the middle flow, and ultimately undergoing further processing in the exit flow. Within the Xception architecture, its 36 convolutional layers are organised into 14 modules. In particular, all of these modules feature linear residual connections, except for the initial and terminal ones. Fig. 1 shows the whole Xception architecture as follows. Compared to other DL architectures, the Xception model has shown advanced performance with a reduced time cost during the training process and has been recorded as the state-of-the-art model in many medical-related tasks (Kassani et al., 2019; Liu et al., 2022).

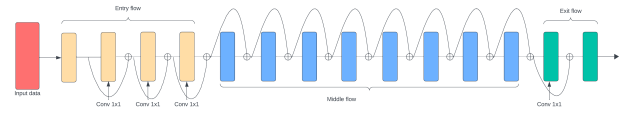


Figure 1: Xception module.

For the SSL setting, we employed ResNet50 architecture (He et al., 2016) since it is also a well-performed model and has been tested with numerous applications. ResNet50 is a 50-layer convolutional neural network (48 convolutional layers, one max pool layer, and one average pool layer). Each convolutional layer uses a bottleneck design for the building block which consists of two 1x1 convolutions as the bottleneck to process the input and output features, reducing the number of parameters and matrix multiplications. The identity mapping used in ResNet allows the model to bypass a CNN weight layer if the current layer is not necessary, which also helps avoid overfitting problems to the training set. The ResNet50 architecture is shown in the following Fig. 2.

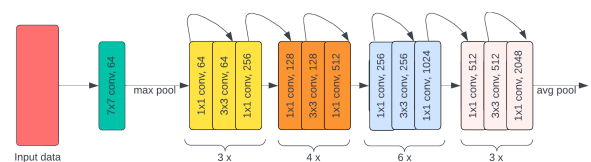


Figure 2: ResNet-50 module.

Both pre-trained methodologies incorporated the Adam optimiser, commencing with an initial learning rate of 0.001 and undergoing 50 epochs during both the pre-training and re-training phases. To enhance the robustness of the learning process and introduce variability into the model, the input data were shuffled to provide randomised samples. Furthermore, a stepwise learning rate schedule was used for the optimiser, implemented to mitigate overfitting, involving a gamma value of 0.2 to decrease the learning rate after 40 epochs. It is noteworthy that, in the TL configuration, an additional fine-tuning step was introduced, involving the unfreezing of the entire model's layers to extract more informative features. In this context, the Adam optimiser began with a learning rate of 0.00001 to prevent rapid overfitting of the entire model. This specific fine-tuning step was omitted

Table 4
Pretext training steps.

	TL setting	SSL setting
- Step 1:	Loading empty Xception model.	Loading the source domain images.
- Step 2:	Loading pretrained ImageNet weight.	Image pre-processing.
- Step 3:	Removing original FC layers.	Loading two empty ResNet50 model.
- Step 4:	Adding new FC layers.	Concatenate two ResNet50 models.
- Step 5:		Loading pretrained ImageNet weight to the first ResNet50 model.
- Step 6:		Freeze the first ResNet model layers.
- Step 7:		Adding a new projection head.
- Step 8:		Training the whole model.

in the SSL setting due to the concatenated model’s extensive layer count, coupled with the limited size of the target datasets, making it impractical to tune all model parameters and potentially leading to overfitting.

3.2.1. Pretext Pretraining Design

For the pre-training stage, we followed a workflow as shown in Fig. 3. The proposed methods start from processing input data and follow their corresponding pre-training setting to get useful pre-trained knowledge before the following retraining and fine-tuning steps. The detailed steps for the two pre-trained methods are presented in Table 4.

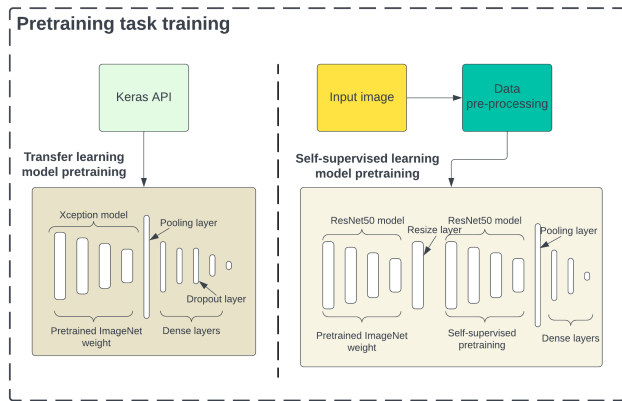


Figure 3: Pretext training workflow diagram.

In the TL setting, we used the Keras library to deploy the Xception model, as it is a high-level API that provides ML and DL models for convenient employment. Additionally, we used the pre-trained ImageNet weight provided by Keras for our Xception model because the ImageNet dataset is one of the representative pre-training datasets and the first choice when applying the TL method. The Xception network import from the Keras library is composed of entry flow, middle flow, exit flow, separable convolution in-depth, and Fully Connected (FC) layers. We also removed the original fully connected layers since it is designed for ImageNet classification tasks and is not useful for our following downstream tasks. Five additional dense layers and one dropout layer were then used to build a custom projection head to prepare for the following training of the downstream task. The dense layers facilitated linear mapping from input to output, incorporating a ReLU activation function to enhance computational efficiency and effectiveness. The dropout layer was designed to randomly set a fraction of

input units to zero during forward and backward passes, mitigating overfitting, particularly vital when working with small datasets or complex models. Notably, the final dense layer was combined with a softmax layer, which produced predictions by assigning the class with the highest probability as the model’s output. By employing these additional fully connected layers, we aim to provide better network performance and reduce overfitting risks.

For the SSL setting, the method we choose to pre-train the model is the Simple Framework for Contrastive Learning of Visual Representations (SimCLR) method (Chen et al., 2020). At the same time, Chen and his colleagues have used ResNet50 as the base model. In our study, the base model is a concatenated model that is combined with two ResNet50 networks. The reason for using a hybrid model is that the selected Xception model for the TL setting has a higher Top-1 and Top-5 accuracy performance than the normal ResNet-50 model on the ImageNet classification task, which states that they might have a performance advantage at the architecture level. We wanted to minimise the performance difference due to architecture itself, since the main goal of this study is to compare the effectiveness of two pre-trained methods. The two ResNet networks were concatenated using two resize layers, as the first ResNet is a pre-trained model using ImageNet weights and the second ResNet is an empty network without any pre-trained weight. The first ResNet has been frozen during the training process and will be treated as a feature extractor. The reason for utilising a network as the feature extractor is to provide well-extracted features as input data for the following network and improve the performance of the whole architecture (Kim et al., 2022). The source data are preprocessed by resizing the image size into 224 pixels by 224 pixels. Later, the whole model was trained with source medical data to gain powerful features from self-contrastive learning. In SimCLR setup, the image pairs are generated internally by the model itself utilising data augmentation techniques including resizing, flipping, zooming, rotating, and brightness and hue changing, serving as pseudo labels for the training data and supporting contrastive loss calculating. Fig. 4 gives a sample of the pseudo-labelled generated.

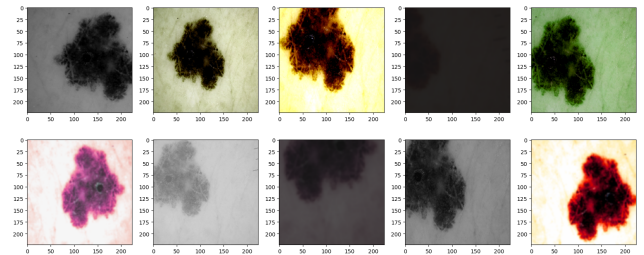


Figure 4: Self-generated pseudo label sample.

The SimCLR method utilised a loss function called NT-Xent to calculate the training loss by contrasting the

representations of positive pairs (similar images) and concurrently creating negative pairs (dissimilar images). The equation of the loss function is as follows.

$$l_{i,j} = -\log \frac{\exp(\text{sim}(z_i, z_j)/\tau)}{\sum_{k=1}^{2N} 1[k \neq i] \exp(\text{sim}(z_i, z_k)/\tau)}$$

The positive pair of example (i,j) uses $1[k \neq i]$ as an indicator function to evaluate if $k \neq i$, and τ denotes a temperature parameter while the final loss is computed by summing all positive pairs and divide by $2 \times N = \text{views} \times \text{batch-size}$. The loss function encourages the model to bring positive pairs closer within the embedding space, while pushing negative pairs further apart, thereby enhancing the learning from input representations. Following the SimCLR method, a projection head containing three linear layers was added to the top of the base ResNet to be trained to maximise agreement using contrast loss. Moreover, we trained two pre-trained SSL models using the grey-scale and colourful medical image datasets, respectively, for the different target domains to reduce the risks of domain mismatch and compare the effectiveness by using ImageNet weight directly. Notably, we used image data from different modalities to enlarge the size of the pre-training data, providing the network with more disease characteristics to learn powerful features.

3.2.2. Downstream training Design

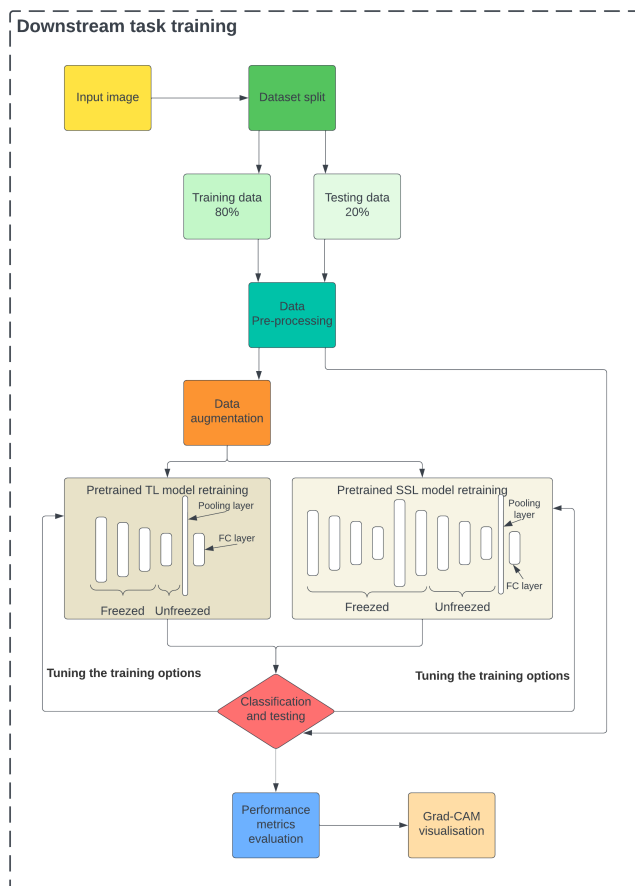


Figure 5: Downstream training workflow diagram.

Table 5

Downstream training steps.

	TL setting	SSL setting
- Step 1:	Loading the target images.	Loading the target images.
- Step 2:	Loading the pre-trained model.	Loading the pretrained model.
- Step 3:	Data split.	Data split.
- Step 4:	Data preprocessing.	Data preprocessing.
- Step 5:	Data downsampling or augmentation.	Data downsampling or augmentation.
- Step 6:	Model retraining & fine-tuning.	Model retraining.
- Step 7:	Model testing.	Model testing.
- Step 8:	Class activation map building.	Class activation map building.

The downstream training process, depicted in Fig. 5, adheres to a systematic workflow. Initially, the data from the target domain were divided into training (80%) and testing (20%) subsets. Subsequently, all data were preprocessed to align with the input specifications of the respective model. The input data has an additional data-altering step using the down-sampling or augmentation technique before the fine-tuning step to address the data imbalance issue. Table 5 lists the working steps for each pre-trained method setting.

Data preprocessing

To facilitate subsequent classification tasks, rigorous data pre-processing was conducted to meet the model's input requirements. The input data were transformed into four dimensions, encompassing batch size, colour channels, height, and width. The batch size determines the number of training examples processed in each iteration, which have been set to 64 in the experiment to prevent memory overflow. The colour channels represent the colour information that the model holds and are based on three base colours 'Red, Green, and Blue. For grey-scale images, which only possess a single colour channel, two pseudo channels were introduced by replicating the original channel. Additionally, height and width dimensions were standardised to 224 pixels by 224 pixels to maintain the consistency of the image. Furthermore, the OneHot encoding technique was applied to convert all labels into vector representations based on their respective categories for the convenience of the following evaluation calculations.

Data down-sampling and augmentation

Data imbalance is a prevalent challenge in the medical domain, manifested when certain classes within the training set exhibit a significantly higher number of examples than others. This occurrence stems from the varying frequencies of different diseases, making it impractical to collect data evenly across all classes in experiments. Previous studies have indicated that such a class imbalance negatively affects the learning process and can decrease the performance of CNN models (Buda et al., 2018). In our investigation, we identified a substantial data imbalance in the BusI and ChestCT datasets. In particular, BusI's first-class benign featured 437 images, twice the count of the second-class malignant (210 images), and three times that of the third-class normal (133 images). To address the imbalance in our target dataset, we implemented two data-altering techniques: data down-sampling and data augmentation.

Table 6
Downsampled target datasets size.

Datasets	Methods	Categories	Samples
BusI	Down-sampling	Train	108 images each class
BusI	Down-sampling	Test	25 images each class
			Total: 399 images
Chest CT	Down-sampling	Train	127 images each class
Chest CT	Down-sampling	Test	32 images each class
			Total: 636 images
Kvasirv2	Down-sampling	Train	100 images each class
Kvasirv2	Down-sampling	Test	25 images each class
			Total: 1000 images
EyePacs	Down-sampling	Train	500 images each class
EyePacs	Down-sampling	Test	100 images each class
			Total: 1200 images

Data down-sampling operates at the data level, randomly removing examples from majority classes until all classes share an equal number of instances (Haixiang et al., 2017). This method aims to create a balance between classes by ensuring that each class has an identical number of examples. In our study, we randomly removed samples from target datasets with oversized classes, equalising the sample count for each class. The sample number for each target dataset down-sampled is listed in Table 6.

Similarly, data augmentation seeks to balance the number of samples in each class by augmenting the minority classes. This method involves randomly selecting samples and replicating them, proven to enhance feature learning and improve model generalisability (Shorten & Khoshgoftaar, 2019). For this experiment, rotation, flip, zoom, and blur methods were applied to the training data, guaranteeing a balanced representation for each class. Table 7 details the augmentation functions and values employed. The rotation function rotates the input images with an angle from -15 to 15 degrees, while the flip function reflects the input images horizontally on the X-axis. The zoom function transforms the input images into 80% of the original size, and the blur function uses the Gaussian function to give an average weight to all pixels in a kernel of 9x9. The original images and the augmented samples are illustrated in the following Fig. 6 to provide a visual representation of the transformation process. Specifically, Table 8 furnishes the post-augmentation size of each class within the target datasets. In the case of the BusI dataset, samples within the malignant class underwent a single round of augmentation utilizing the mixed function, while samples in the normal class underwent three rounds of augmentation through rotation, blur, and mixed functions to align with the sizes of other classes. The chest CT dataset, characterised by an adenocarcinoma class with a surplus of samples compared to other classes, underwent mixed augmentation functions for the remaining three classes (large.cell.carcinoma, normal, and squamous.cell.carcinoma) to harmonise their sizes. For the balanced Kvasirv2 and EyePacs datasets, each of their classes was subjected to one round of mixed augmentation to maintain the equilibrium of the dataset.

Table 7
Augmentation functions.

Function	Value	Action
Rotation	[-15 to 15]	Rotating input data by -15 to 15 degrees
Flip	1	Randomly flip input data horizontally and vertically
Zoom	0.8	Zoom in by 0.8 distance from the middle
Blur	[9,9]	Blur the input data with a 9x9 pixel kernel
Mixed	-	Rotating and flipping input data at the same time

Table 8
Augmented target datasets size.

Datasets	Methods	Categories	Samples
BusI	Augmentation	Train	397 images in Benign class
BusI	Augmentation	Train	340 images in Malignant class
BusI	Augmentation	Train	372 images in Normal class
BusI	Augmentation	Test	40 images each class
			Total: 1229 images
Chest CT	Augmentation	Train	281 images in Adenocarcinoma class
Chest CT	Augmentation	Train	236 images in LargeCellCarcinoma class
Chest CT	Augmentation	Train	228 images in Normal class
Chest CT	Augmentation	Train	207 images in SquamousCellCarcinoma class
Chest CT	Augmentation	Test	45 images each class
			Total: 1132 images
Kvasirv2	Augmentation	Train	1600 images each class
Kvasirv2	Augmentation	Test	200 images each class
			Total: 14400 images
EyePacs	Augmentation	Train	5000 images each class
EyePacs	Augmentation	Test	500 images each class
			Total: 11000 images

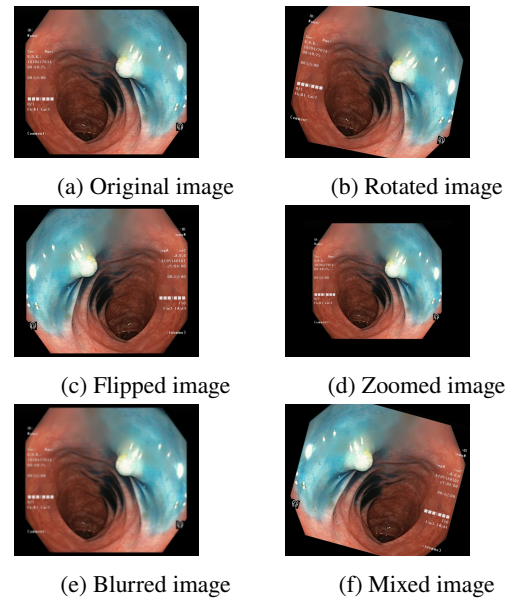


Figure 6: The augmented image sample.

Although these data-altering methods have been proven to be effective in addressing data imbalance, some concerns should be paid attention. Data down-sampling risks the loss of valuable information and exacerbates the data scarcity problem, particularly given the relatively small sizes of our target datasets. Data augmentation, on the other hand, poses a risk of overfitting due to the repetition of samples, potentially capturing certain features excessively over time. To comprehensively evaluate the impact of these data-altering methods across two pre-trained methods, we extended our experiment to apply data down-sampling and augmentation

universally, even in the dataset absent of apparent data imbalance issues.

Model retraining and fine-tuning

In the retraining phase, the initial step involved retraining select layers, particularly the fully connected layers, to leverage knowledge from pre-trained parameters and learn from the new target data. The majority of the model's layers were kept frozen, with only the top layers and the fully connected layer adapting to the target data. Balancing the retraining of layers was crucial, as an excessive number of retrained layers might compromise the model's generalisation and reliability. Various settings of the number of unfreezing layers were tested to strike a balance. This methodology ensured the preservation of most transferred knowledge while allowing a few layers to adapt to unique features from input images, assessing the effectiveness of pre-trained weights from TL and SSL settings. Additionally, the Adam optimiser and cross-entropy loss function were uniformly applied to both models, ensuring comparability and alignment with nonbinary downstream tasks.

During the fine-tuning phase, we systematically unfroze all layers in the chosen model and fine-tuned the entire model with a conservative learning rate for an additional 30 epochs. After each epoch, the model assessed its training accuracy and loss, dynamically adjusting the learning rate if the training loss plateaued for three consecutive epochs. This iterative process was designed to meticulously optimise the model's parameters throughout all layers, enhancing the alignment of learnt features with the characteristics of the target domain.

Model testing

After the retraining and fine-tuning stages, the pre-trained model acquired substantial knowledge for subsequent downstream tasks. In the testing phase, we used ground-truth images extracted from the target dataset to evaluate the performance of the trained models. Given the focus of this study on medical classification tasks, each test image underwent model predictions for their respective categories. The accuracy, loss, sensitivity, precision, and F1 score metrics were computed for each prediction, serving as key indicators for the subsequent analysis.

Class activation heat-map development

The final step involves the generation of feature visualisation heat-maps, elucidating the decision-making process of the trained model, and assessing its reliability. Feature visualisation is valuable for uncovering and understanding the learnt features within DL models. Zhou et al. (2016) introduced the Class Activation Mapping (CAM) method, which incorporates a global average pooling layer into a standard CNN. This innovation facilitated the identification of critical feature contributions linked to CNN's specific predictions, shedding light on the rationale behind the model's decisions. Furthermore, Selvaraju et al. (2017) introduced

Gradient Weighted Class Activation Mapping (Grad-CAM), using gradients from the network's final convolutional layer to generate a coarse localisation map. This map highlights influential regions within an image that contribute to the prediction of specific concepts or classes. In our study, we embraced the Grad-CAM technique on the model's final layer to generate class-specific heat-maps. The objective is to unveil evidence of how the models arrive at predictions, with the heat-maps delineating regions of significance in the model's prediction rationale.

4. Experimental Evaluation

This section evaluates the test results of the fine-tuned model on the target domain. The proposed methods are run in Python 3.10.12 on a Windows 11 pro system, under a desktop PC equipped with an Intel (R) Core (TM) i5-12600K CPU at 4.8 GHz, an NVIDIA Geforce RTX 4080 GPU, and 64 GB of RAM. In this study, one TL model was downloaded and utilised pre-trained ImageNet weight from the Keras library and two SSL models were pre-trained on two groups of colourful and grey-scale medical image datasets.

4.1. Evaluation Metrics

The statistical metrics for evaluating classification performance can be various, and we have used some of the most common methods including Accuracy, Loss, Sensitivity (Recall), Precision and F1 score. The calculation equations of these performance measurements are shown as follows. The TP here means true positive, TN is true negative, and they represent the number of correctly classified negative and positive instances, respectively. The FP is false positive, and FN stands for false negative, which denotes the number of misclassified positive and negative cases, respectively.

$$Accuracy = \frac{TN + TP}{TN + FN + TP + FP}$$

$$CrossEntropy - Loss = - \sum_{c=1}^M y_{o,c} \log(p_{o,c})$$

$$Sensitivity = Recall = \frac{TP}{TP + FN}$$

$$Precision = \frac{TP}{TP + FP}$$

$$F1 = 2 * \frac{Precision * Recall}{Precision + Recall}$$

4.2. Experimental assessment

This section intricately elucidates the performance dynamics exhibited by the proposed pre-trained CNN models, namely Xception and concatenated ResNet, across both the training and testing phases. The comprehensive evaluation entails a meticulous comparison of the two pre-trained models, encompassing their performance across various training phases, multiple fine-tuning steps, combined with data

Table 9

Results of TL model on training set.

Datasets	Acc(%)	Loss	Sen(%)	Pre(%)	F1(%)
BusI	84.23	0.41	74.69	82.00	77.02
BusI (Augmented)	96.94	0.09	97.72	97.63	97.67
BusI (Down-sampled)	63.85	0.84	56.78	64.13	55.05
Chest CT	96.72	0.10	95.58	95.63	95.44
Chest CT (Augmented)	98.42	0.07	98.83	98.88	98.86
Chest CT (Down-sampled)	88.30	0.48	88.28	88.14	87.92
Kvasirv2	95.17	0.13	96.71	96.77	96.70
Kvasirv2 (Augmented)	99.93	0.08	99.99	99.99	99.99
Kvasirv2 (Down-sampled)	100	0.01	100	100	100
EyePacs	99.78	0.01	99.72	99.71	99.71
EyePacs (Augmented)	99.95	0.01	99.96	99.94	99.94
EyePacs (Down-sampled)	99.36	0.01	100	99.50	99.50

Table 10

Results of SSL model on training set.

Datasets	Acc(%)	Loss	Sen(%)	Pre(%)	F1(%)
BusI	98.29	0.57	90.28	91.89	83.59
BusI (Augmented)	99.00	0.56	98.97	99.05	99.00
BusI (Down-sampled)	99.21	0.56	91.60	91.68	92.25
Chest CT	99.83	0.74	99.83	99.78	99.80
Chest CT (Augmented)	99.58	0.74	96.75	97.08	96.88
Chest CT (Down-sampled)	99.80	0.74	95.74	95.90	95.84
Kvasirv2	93.76	1.33	85.00	84.86	84.96
Kvasirv2 (Augmented)	91.00	1.36	84.35	84.41	84.30
Kvasirv2 (Down-sampled)	99.39	1.28	91.98	92.13	91.79
EyePacs	98.18	0.33	92.12	92.10	92.10
EyePacs (Augmented)	98.43	0.32	93.00	93.03	93.02
EyePacs (Down-sampled)	98.53	0.32	93.10	93.13	93.10

down-sampling, augmentation and double fine-tuning techniques, juxtaposition with state-of-the-art models operating on the same target datasets, and scrutiny under the lens of XAI techniques. Within the scope of these comparative analyses, salient metrics such as performance metrics, generalisability, temporal considerations, and robustness were systematically scrutinised. This rigorous examination aims to present a nuanced understanding of the inherent strengths and weaknesses encapsulated within the two pre-trained methods.

Comparison in training phase assessment

The performance of the training stage for each model is presented and tabulated in Tables 9 and 10. When faced with grey-scale datasets, the TL model achieved an accuracy of 84.23% and 96.72% on the base BusI and Chest CT datasets, respectively, which is relatively lower than the performance of the SSL model at 98.29% and 99.83%. The SSL model

exhibited higher sensitivity, precision, and F1 scores on BusI (90.28%, 91.89%, and 83.59%) and Chest CT (99.83%, 99.78%, and 99.8%), showcasing a 20% improvement over the TL model on these two datasets. Additionally, the performance of the TL model in the down-sampled BusI and chest CT datasets experienced a significant drop from 84.23% to 63.85% and from 96.72% to 88.3%, respectively. In contrast, the SSL model maintained stable results even with reduced training samples, achieving training accuracies of 99.21% and 99.8% on down-sampled datasets, without any reduction from the base datasets. Notably, the augmentation method salvaged the TL model from this unfavourable situation, significantly improving accuracy from 84.23% to 96.94% and 96.72% to 98.42%, aligning sensitivity, precision, and F1 scores with the SSL model. At the same time, the performance of the SSL model on augmented datasets remained high at 99% and 99.58%, maintaining parity with the base dataset.

Conversely, the situation reversed in colourful datasets. The TL model demonstrated commendable performance, achieving 95.17% accuracy, 96.71% sensitivity, 96.77% precision, and 96.7% F1 score on the base KvasirV2 dataset. In comparison, the SSL model exhibited lower accuracy at 93.76% and poorer performance in sensitivity (85%), precision (84.86%), and F1 score (84.96%). Surprisingly, the TL model achieved perfect scores of 100% accuracy, sensitivity, precision, and F1 score with the down-sampled dataset, while the SSL model showed a consistent trend in each evaluation metric. This scenario is attributed to the larger scale of the KvasirV2 dataset compared to grey-scale datasets, requiring more time for the model to assimilate features and can not reach a suitable gradient within 50 epochs. Thus, the down-sampling method expedited the model's adaptation to target representations by reducing the total dataset size. Furthermore, the performance of the SSL model in the augmented dataset supported this assumption, with a drop in accuracy from 93.76% to 91% compared to the original dataset due to the increasing amount of learning samples. For the EyePacs dataset, the TL model also demonstrates superior performance compared to the SSL model. The TL model achieves 99.78%, 99.95%, and 99.36% accuracy across the base, augmented, and down-sampled versions of the EyePacs dataset, which is 1.5% higher than the SSL model in base and augmented versions, and 0.8% higher in the downsampled dataset. Neither the augmentation nor down-sampling techniques have significantly impacted the performance of the TL and SSL models, as the general performance of both models in the EyePacs dataset remains high and stable. Compared to the other three datasets, the main difference lies in the EyePacs dataset having only two classes, and the downstream task for this dataset is binary classification, making it easier to learn enough features than other datasets. The experimental results show a small performance advantage of the TL method compared to the SSL method in colourful target datasets.

Summarising the training stage performance of both pre-trained models, the SSL model demonstrates superior performance with grey-scale datasets, while the TL model excels with colourful datasets. Additionally, the results underscore the positive impact of the augmentation technique on pre-trained model performance, but it is noteworthy that the training time and computational resource costs of the augmented datasets also raised as the training sample number increased. In contrast, the down-sampling technique demonstrates opposing effects mainly on grey-scale datasets. It enhances the TL model's performance on colourful datasets but diminishes it on grey-scale datasets, revealing the sensitivity of the TL method to dataset size reduction, particularly in smaller datasets like BusI and Chest CT (with less than 800 samples). The performance improvement observed in the relatively large colourful KvasirV2 dataset (with 8000 samples) and EyePacs (with 6000 samples) suggests that the pre-trained TL model could perform stably when the target dataset is reasonably substantial. However, the poor performance of the down-sampling method poses a risk

of losing critical information and increases susceptibility to overfitting, which should raise attention in subsequent experiments.

Comparison in testing phase assessment

The performance evaluation of the two pre-trained models during the testing phase is encapsulated in Table 11 and Table 12. Moreover, Fig. 7, Fig. 8, Fig. 9, and Fig. 10 provide a visual representation of the confusion matrix for the original, augmented, and down-sampled target datasets, facilitating a comparison between predicted and true labels across each class. The assessment metrics were derived from the confusion matrix values, which provided a detailed breakdown of the model classifications. From the table, the testing outcomes of the grey-scale datasets follow the trends observed in the training phase, revealing the SSL model's superior performance on these datasets. Specifically, the TL model achieved an accuracy of 69.2% on the BusI dataset and 74% on the Chest CT dataset. In contrast, the SSL model attained accuracy rates of 74.16% and 93.02% and showcased a 10% advantage in each sensitivity, precision, and F1 score metric. Also, the SSL model combined with both augmentation and down-sampling techniques showed a more balanced performance distribution between each class from the confusion matrix, demonstrating their ability to address data imbalance issues, while the TL model only had improvements when combined with the augmentation technique.

However, same as the training phase, the down-sampling technique led to a reduction in performance for both pre-trained models on the grey-scale testing set. The decrease for the TL model on down-sampled datasets ranged from 5% to 10%, emphasizing a noteworthy performance decline of the down-sampling technique when facing imbalanced small datasets. Comparatively, the SSL model also experienced a performance decrease, albeit at a smaller rate of about 2% compared to the base dataset performance. Given the SSL model's stable performance when facing reduced input samples during the training stage, it exhibits greater resilience to sample reduction, demonstrating superior efficacy in handling small datasets compared to the TL model. On the other hand, the augmentation technique proved beneficial for both pre-trained models, with the TL model displaying more substantial improvement, ranging from 69.2% accuracy to 77.5% on BusI and 74% to 93.3% on Chest CT. This observation aligns with the earlier finding that the TL model is more sensitive to the target dataset size, while the SSL model is less sensitive to the dataset size but also benefits from its increase. Furthermore, the correctly predicted ratio of the augmented BusI dataset's Malignant and Normal class increased from 53% and 60% to 72%, and the prediction performance of the Large.cell and Squamous.cell classes of the augmented Chest CT dataset improved from 80% to 90%. This underscores the augmentation technique's benefits in facilitating a more reasonable result and reducing the impact of imbalanced datasets.

Table 11
Results of TL model on testing set.

Datasets	Acc(%)	Loss	Sen(%)	Pre(%)	F1(%)
Bus1	69.20	0.75	69.16	79.21	69.28
Bus1 (Augmented)	78.30	1.18	82.49	82.66	77.51
Bus1 (Down-sampled)	64.00	0.91	64.00	69.17	64.19
Chest CT	87.30	0.67	86.60	90.20	88.11
Chest CT (Augmented)	93.30	0.26	93.32	93.69	93.39
Chest CT (Down-sampled)	62.50	1.43	88.28	88.14	87.92
Kvasirv2	91.50	0.22	90.90	91.00	90.87
Kvasirv2 (Augmented)	93.40	0.38	93.37	93.37	93.35
Kvasirv2 (Down-sampled)	70.50	1.89	70.50	71.28	70.65
EyePacs	92.10	0.30	92.10	92.00	92.00
EyePacs (Augmented)	91.20	0.80	91.10	91.10	91.00
EyePacs (Downsampled)	88.00	0.66	88.00	88.38	87.90

Table 12
Results of SSL model on testing set.

Datasets	Acc(%)	Loss	Sen(%)	Pre(%)	F1(%)
Bus1	74.16	0.80	74.16	79.58	73.71
Bus1 (Augmented)	81.66	0.73	81.66	84.05	81.72
Bus1 (Down-sampled)	72.00	0.79	72.00	73.48	71.88
Chest CT	93.02	0.81	94.18	93.03	93.42
Chest CT (Augmented)	97.22	0.77	97.21	97.22	97.20
Chest CT (Down-sampled)	91.40	0.82	91.40	91.49	91.23
Kvasirv2	82.93	1.44	82.93	83.03	82.89
Kvasirv2 (Augmented)	85.81	1.41	85.81	82.96	84.36
Kvasirv2 (Down-sampled)	78.00	1.47	78.00	77.80	77.76
EyePacs	83.10	0.47	83.10	83.10	83.00
EyePacs (Augmented)	83.20	0.48	83.20	83.20	83.20
EyePacs (Downsampled)	75.50	0.54	75.50	75.50	75.50

In the context of colourful datasets, the TL model demonstrated superior performance across all evaluation metrics, achieving an impressive 91.5% accuracy on the KvasirV2 dataset and 92.1% accuracy on the EyePacs dataset, maintaining a 10% performance advantage over the SSL model. However, the TL model experienced a notable decline on the KvasirV2 dataset when employing the down-sampling technique, resulting in a decrease of about 20% in accuracy, sensitivity, precision, and F1 score compared to the performance on the base KvasirV2 dataset. In contrast, the SSL model exhibited a slight decrease of 5% across each evaluation metric. This situation likely arose due to the greater reduction range of the KvasirV2 dataset compared to the other two grey-scale datasets and the TL model's sensitivity towards dataset size. However, the decrease in performance of the TL model on EyePacs is much smaller,

which can be attributed to the complexity difference between the classification tasks in the KvasirV2 and EyePacs datasets.

Notably, there is no indication that the down-sampling technique benefits in narrowing the performance gap between the classes, and it may even deepen the gap, especially in datasets like KvasirV2 due to reduced information from the samples. Compared to the significant performance improvement in grey-scale datasets, the augmentation technique contributed only modest improvements to the test results of both the KvasirV2 and EyePacs datasets, with the TL model improving by 2% and the SSL model by 3% within each evaluation metric on KvasirV2, and no improvement for either TL or SSL models on EyePacs. This discrepancy may stem from the original size of the KvasirV2 and EyePacs datasets being sufficiently large for the models to learn robust features, thereby limiting the incremental value of further dataset size augmentation. However, despite

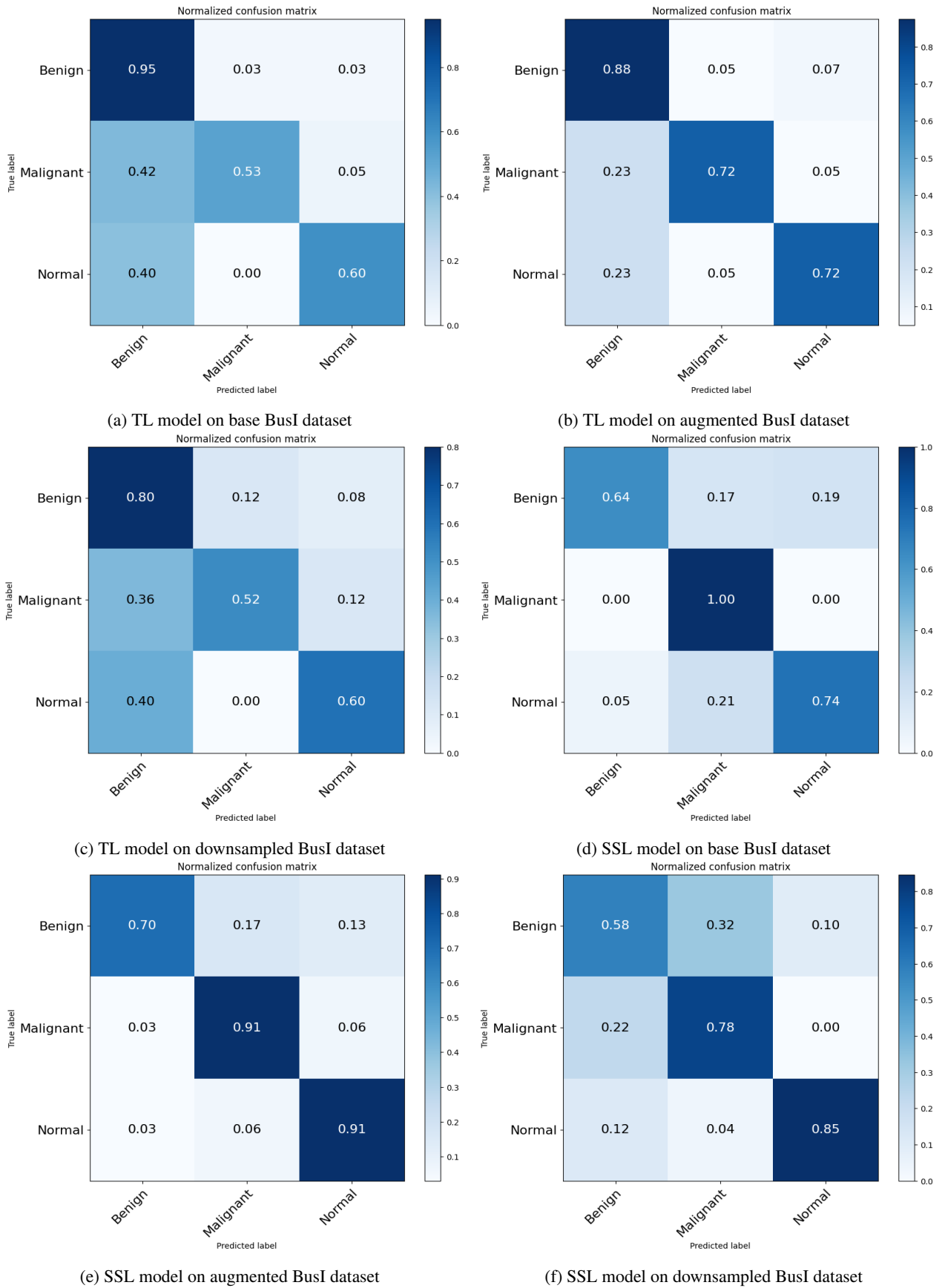
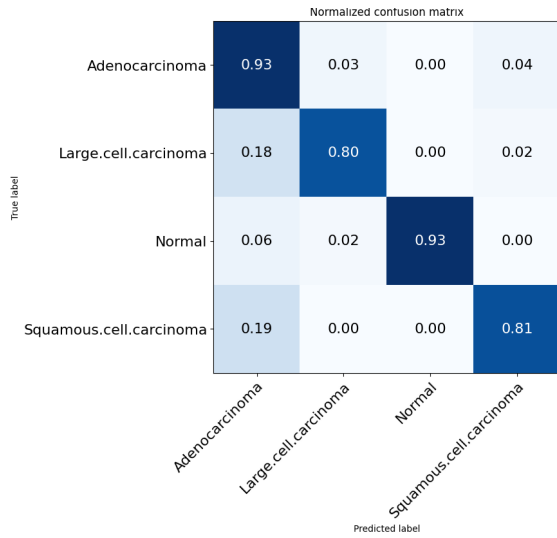
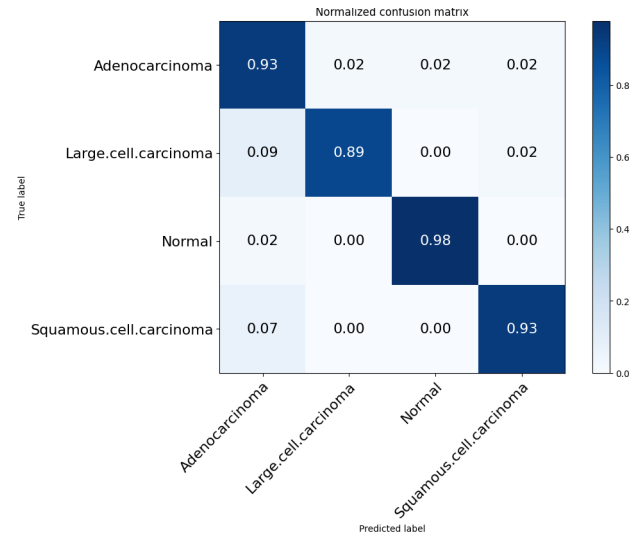


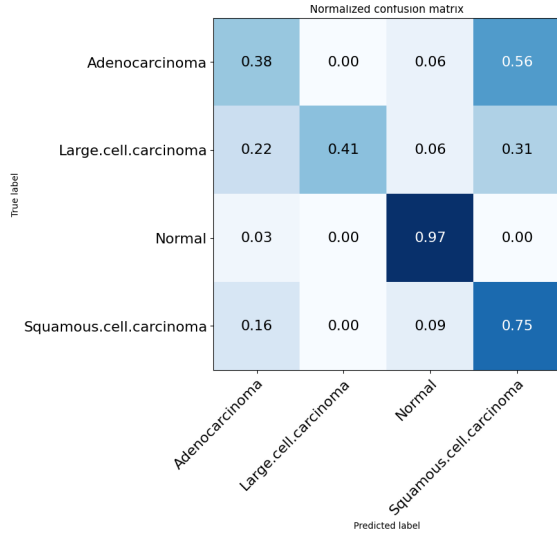
Figure 7: Confusion matrix (a), (b), (c) represent TL model on BusI dataset, Confusion matrix (d), (e), (f) represent SSL model on BusI dataset.



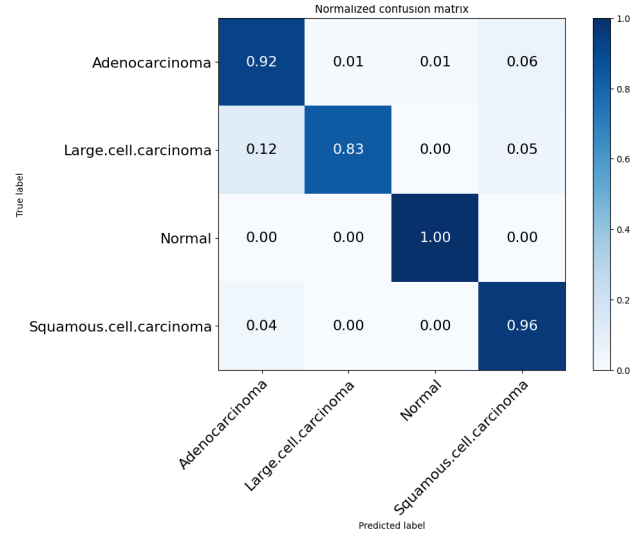
(a) TL model on base ChestCT dataset



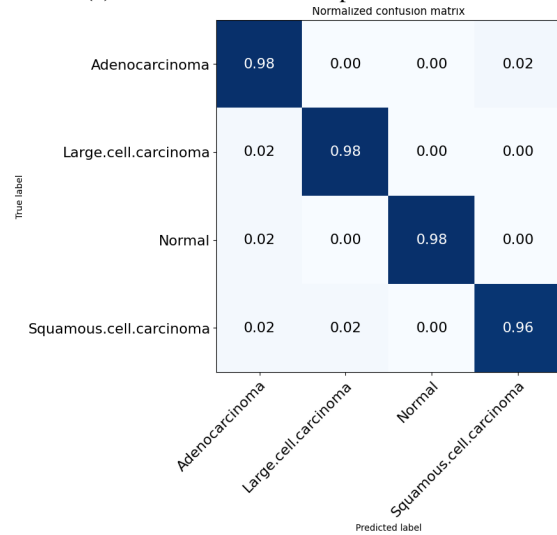
(b) TL model on augmented ChestCT dataset



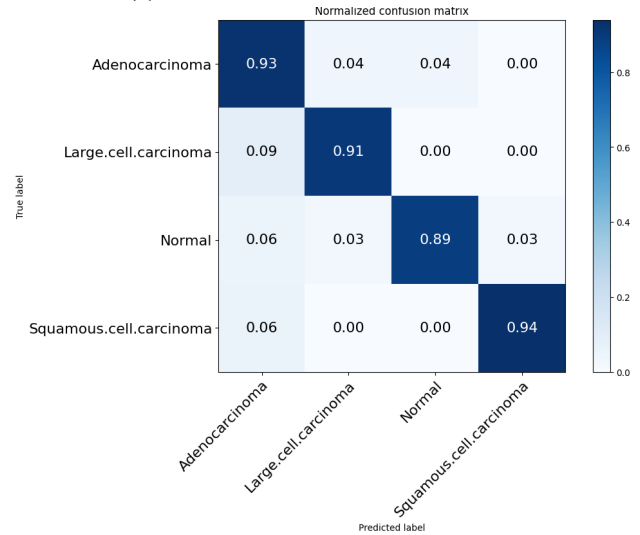
(c) TL model on downsampled ChestCT dataset



(d) SSL model on base ChestCT dataset

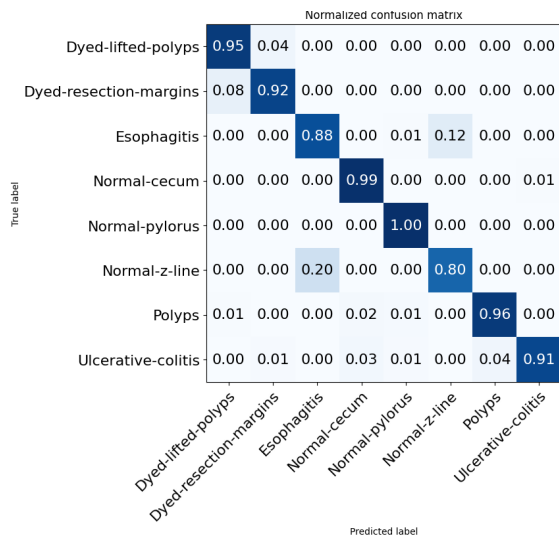


(e) SSL model on augmented ChestCT dataset

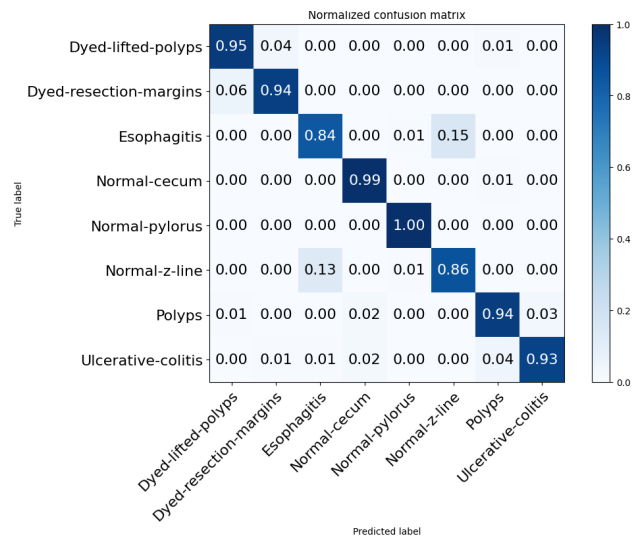


(f) SSL model on downsampled ChestCT dataset

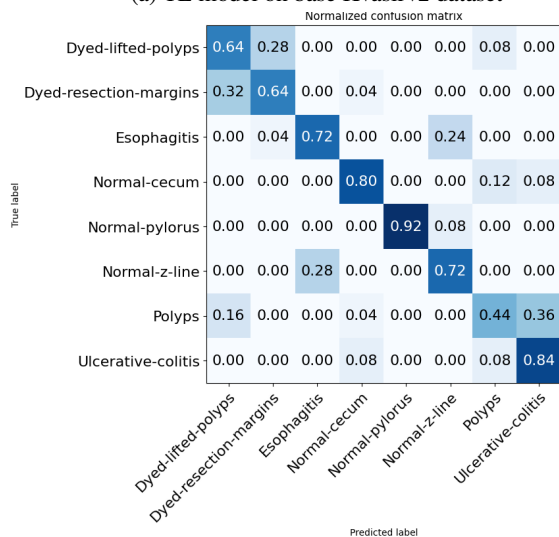
Figure 8: Confusion matrix (a), (b), (c) represent TL model on ChestCT dataset, Confusion matrix (d), (e), (f) represent SSL model on ChestCT dataset.



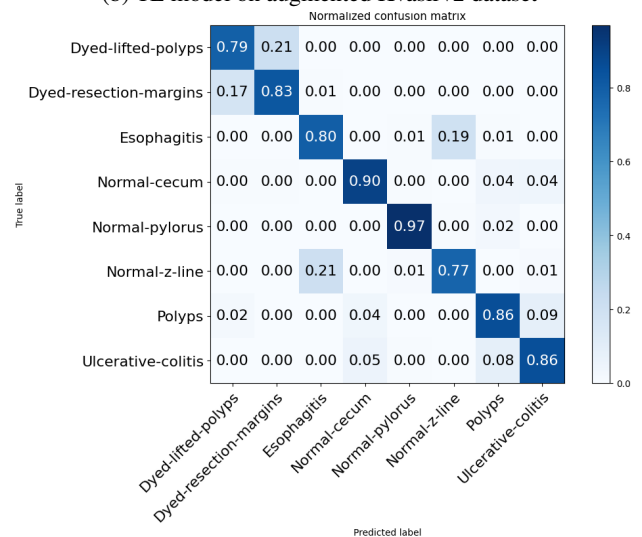
(a) TL model on base Kvasirv2 dataset



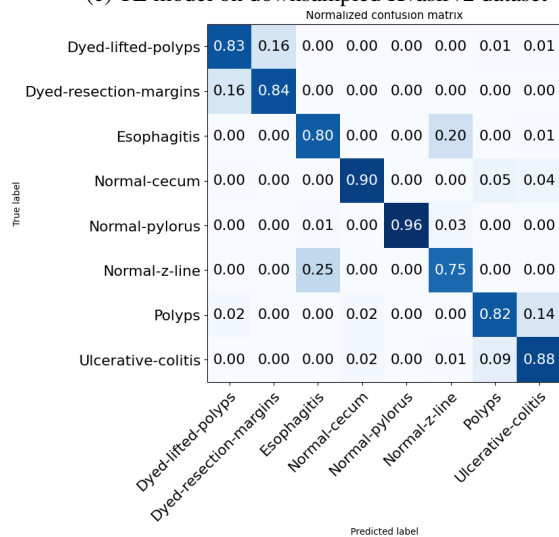
(b) TL model on augmented Kvasirv2 dataset



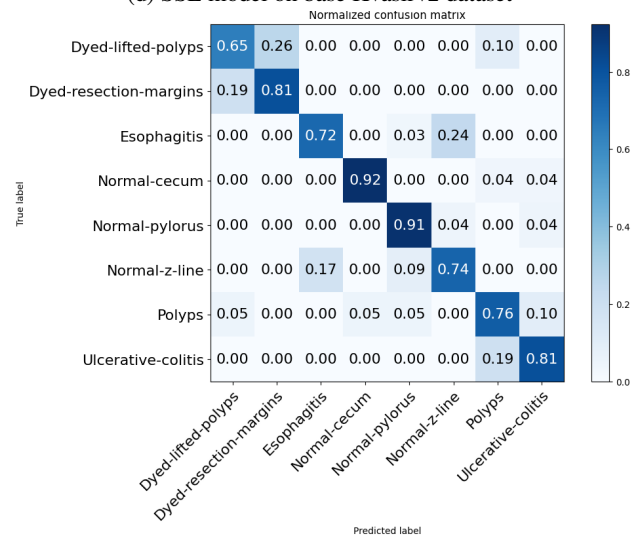
(c) TL model on downsampled Kvasirv2 dataset



(d) SSL model on base Kvasirv2 dataset



(e) SSL model on augmented Kvasirv2 dataset



(f) SSL model on downsampled Kvasirv2 dataset

Figure 9: Confusion matrix (a), (b), (c) represent TL model on Kvasirv2 dataset, Confusion matrix (d), (e), (f) represent SSL model on Kvasirv2 dataset.

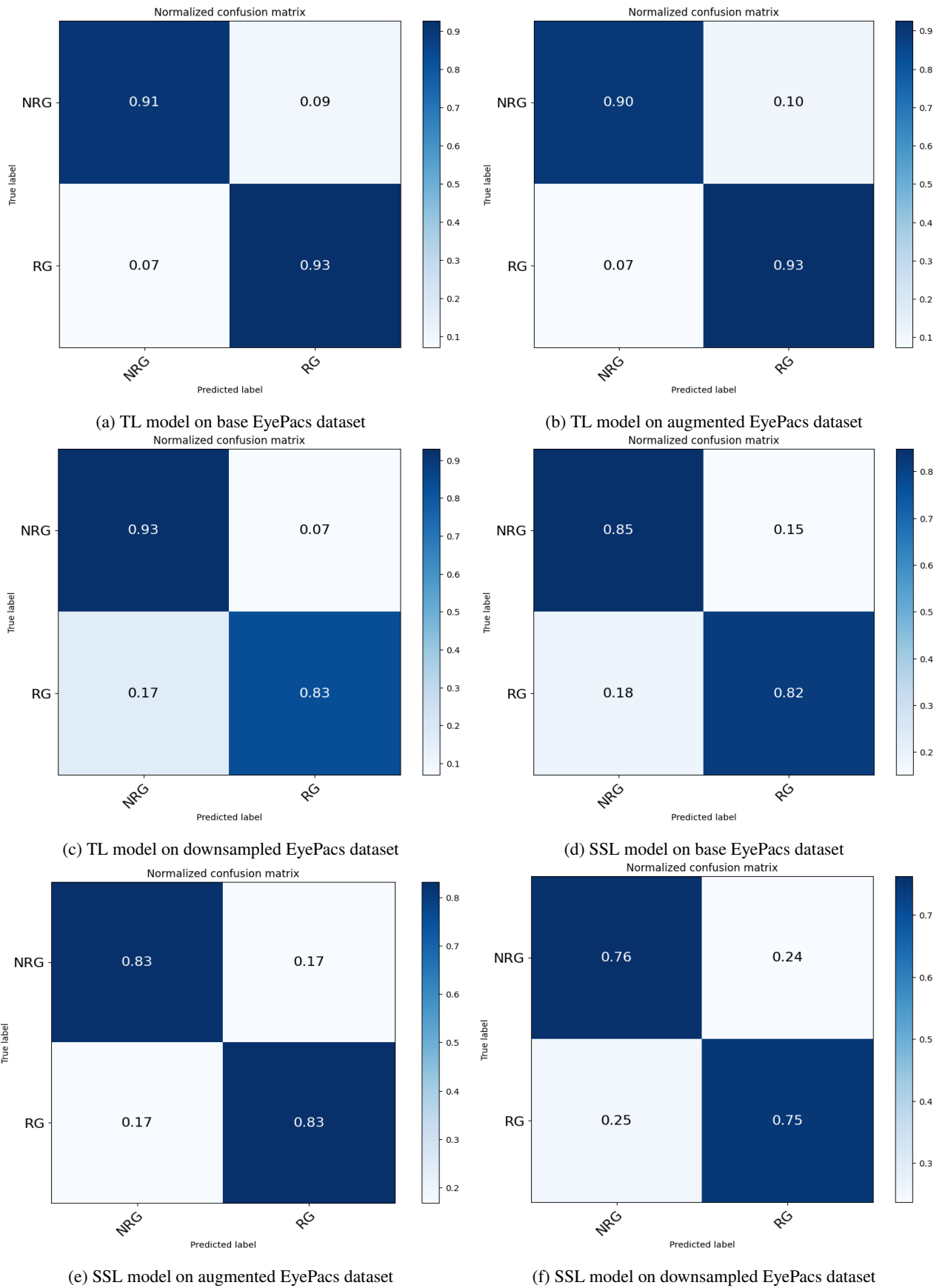


Figure 10: Confusion matrix (a), (b), (c) represent TL model on EyePacs dataset, Confusion matrix (d), (e), (f) represent SSL model on EyePacs dataset.

the limited improvement in the augmentation technique on the TL model in general, it has still shown benefits in reducing the imbalance between each class's performance. For instance, the positive prediction ratio of Esophagitis and Normal-z-line in the original KvasirV2 dataset is 88% and 80%, resulting in an 8% performance gap, highlighting the challenge for the TL model in distinguishing them. Conversely, the performance in the augmented KvasirV2 dataset is 84% against 86%, demonstrating a reduced 2% gap and indicating improvement in the pre-trained model's ability to recognize representations from two classes. A similar trend is observed in the confusion matrix of the SSL model on the base and augmented KvasirV2 dataset, with a reduction in the performance gap between the first and second classes, and the third and sixth classes.

In summary, the performance trends of the two pre-trained models during the testing stage align with the observations made in the training stage. The TL method excels at handling colourful datasets, while the SSL method demonstrates superior performance in grey-scale datasets. One primary reason for this divergence lies in the utilisation of ImageNet weight in the pre-trained TL model, while leveraging the colourful dataset's knowledge can improve the ability to handle colourful target datasets. However, this explanation does not fully account for the SSL model's comparatively poorer performance on colourful datasets, despite utilizing the pretext colourful medical datasets in the pre-training stage. We posit that the distinctive learning methods of the TL and SSL approaches contribute to this outcome, with recent studies (Ericsson et al., 2021) suggesting that supervised learning settings adeptly glean knowledge from colourful features and outperform unsupervised learning settings. Furthermore, the testing stage results underscore that the SSL model outperforms the TL model in handling smaller datasets, a critical consideration in the medical field where data scarcity issues are prevalent. Importantly, the data down-sampling technique can harm the pre-trained model's performance, especially when the target dataset size is limited, while the data augmentation technique can bring benefits to pre-trained models. However, there is a diminishing effect when applying the augmentation technique to relatively large target datasets.

Comparison with double fine-tuned model

The preceding section provided a comparative analysis of TL and SSL models across both training and testing phases, revealing distinct advantages inherent in each method when applied to grey-scale and colourful medical datasets. Despite leveraging pre-trained knowledge to enhance downstream task learning, the test results sometimes fell short of expectations with the fine-tuned models. For instance, the SSL model failed to achieve satisfactory performance on the BusI dataset initially when a significant portion of the pre-trained model layers was frozen, with only 10% of the top layers being retrained. This scenario improved considerably when most of the layers were unfrozen. When leaving only 25% of the bottom layers' parameters

untouched, there is an enhancement across all evaluation metrics. Similar situations occurred with the TL model on the KvasirV2 dataset. By using a smaller portion of transferred parameters and retraining more layers, the TL model exhibited improved performance on the target dataset. Notably, considering both the BusI and Chest CT datasets being grey-scale and multi-class, the proposed SSL model only achieved optimal performance on the Chest CT dataset. This discrepancy may be attributed to differences in feature distribution between the learned target samples and the transferred weights, indicating a significant role of positive knowledge transfer in the downstream task performances. The initial experimental setup for the pre-trained SSL model involved selecting three grey-scale medical datasets from diverse modalities (MRI, X-ray, and CT) as source data to augment the feature set available to the pre-trained model. The Chest CT dataset showed closer alignment with the source data in feature distribution, while the BusI dataset samples exhibited distinct representations from the source domain data. Furthermore, the pre-trained ImageNet weights did not share similar features with gastrointestinal images, possibly contributing to the performance drop for pre-trained models in both the BusI and KvasirV2 datasets.

As supported by prior pre-training studies (Krishnan et al., 2022), the disparity in representations between the source and target domains significantly influences the success of knowledge transfer. To address the domain mismatch issue to mitigate the impact of domain discrepancy and enhance the SSL and TL models' performance on the BusI and KvasirV2 datasets, we implemented a solution employing the double fine-tuning technique. This approach entails fine-tuning the pre-trained foundational model on an extensive training dataset, followed by further fine-tuning on the specific domain/task with limited training data. For the SSL setting, the pre-trained SSL model using grey-scale knowledge underwent double fine-tuning on an ultrasound dataset called Polycystic Ovary Syndrome (PCOS) (Anagha & Aishwarya, 2021). The PCOS dataset has 3856 ultrasound images and was categorized into infected and non-infected classes. This dataset shares the same imaging technique as the BusI dataset but involves different disease types for detection. Initial fine-tuning involved unfreezing 90% of the pre-trained SSL model layers, followed by using the SimCLR self-supervised learning method to fine-tune the model. Subsequently, an additional fine-tuning phase was conducted on the target BusI dataset, using the same learning settings as the aforementioned experiment to assess performance.

The results, detailed in Table 13, and the evaluation metrics depicted in Fig 11, indicate a significant enhancement in the performance of the double fine-tuned SSL model across all versions of the target dataset compared to the single fine-tuned model. Accuracy and sensitivity on the base dataset notably increased from 74.16% to 79.16%, with precision and F1 score performances improving by 4% and 5.5%, respectively. Similar improvements were observed in both augmented and down-sampled datasets, maintaining a consistent enhancement of approximately 5% across

Table 13

Results of double fine-tuned SSL model on Busl testing set.

Datasets	Acc(%)	Loss	Sen(%)	Pre(%)	F1(%)
Busl	79.16	0.76	79.16	83.36	79.23
Busl (Augmented)	90.00	0.65	90.00	90.21	90.00
Busl (Down-sampled)	77.33	0.79	77.33	80.37	76.76

Table 14

Results of double fine-tuned TL model on KvasirV2 testing set.

Datasets	Acc(%)	Loss	Sen(%)	Pre(%)	F1(%)
KvasirV2	96.40	0.40	96.43	96.44	96.43
KvasirV2 (Augmented)	95.90	0.41	95.87	95.80	95.87
KvasirV2 (Down-sampled)	93.50	0.52	93.50	93.67	93.48

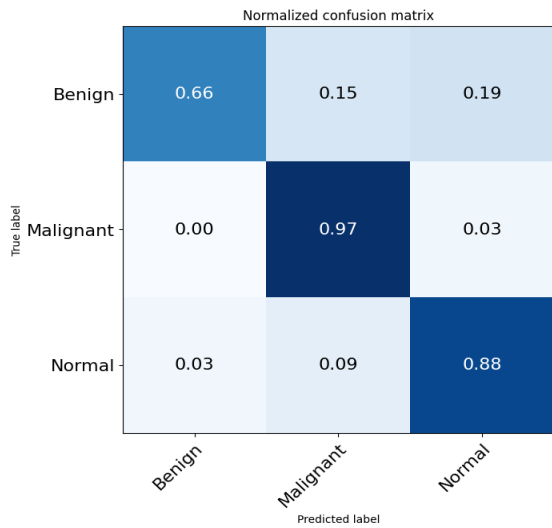
all evaluation metrics. Furthermore, the confusion matrix maps demonstrate improvements in each class and a reduced performance gap between classes, indicating that the pre-trained model has improved its ability to recognize breast tumours from ultrasound images. This outcome highlights that leveraging a related domain dataset for double fine-tuning can significantly enhance the pre-trained model's performance, negating the need for an extensive sample size. Moreover, the conclusion emphasizes that merely enriching the modalities and size of the pre-trained datasets during the pre-training stage may not yield benefits and could potentially waste computational resources. The pivotal factor lies in transferring useful and pertinent knowledge to the target domain to sustain high-performance levels of the pre-trained model.

To assess and compare the effectiveness of the double fine-tuned technique with the TL method, we replicated the process using our pre-trained TL model. The dataset selected for double fine-tuning is known as Medico-2018 (Pogorelov et al., 2018), comprising 14,033 gastrointestinal images. Among these, 5,293 images from the training set were annotated by experienced endoscopists into 16 classes of gastrointestinal diseases, while the remaining 8,740 images from the testing set remained unlabeled. Notably, the Medico-2018 dataset displays significant class imbalances, with notable differences in sample counts across each class. During the first fine-tuning phase, we exclusively utilized the 5,293 annotated images due to the supervised learning approach employed in the pre-trained TL model. We integrated the same projection head, consisting of four dense layers and one dropout layer, as in the previous experiment setting for the TL model to facilitate the supervised learning process. Upon completing the initial training step, the projection head was removed, and the fine-tuned Xception model was applied to the target Kvasirv2 dataset for the second fine-tuning step. This second fine-tuning step followed the same process as before, and the double fine-tuned model underwent testing on the Kvasirv2 dataset for subsequent analysis.

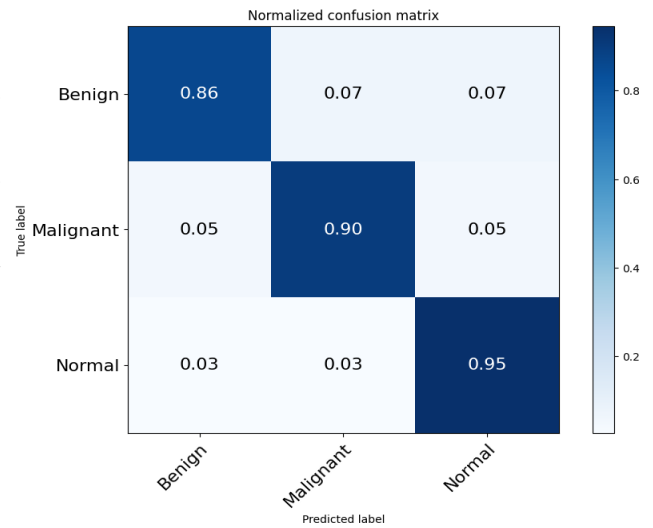
The results of the double fine-tuned TL model are detailed in Table 14, with the corresponding confusion matrix outlined in Fig 11. A noticeable performance improvement is observed in the double fine-tuned TL model compared to the pre-trained TL model. Specifically, the double fine-tuned model demonstrated a 5% enhancement on the base dataset and a 3% improvement on the augmented dataset across metrics such as accuracy, sensitivity, precision, and F1 score. Furthermore, the double fine-tuned model on the base dataset outperformed its counterpart on the augmented dataset. Given the size of the Kvasirv2 dataset, we suggest that this phenomenon occurs because the enriched parameters transferred from the source domain have reduced the requirement of needed features to be learned in the target dataset, thereby providing satisfactory performance. Importantly, the performance of the double fine-tuned TL model on the down-sampled Kvasirv2 dataset witnessed a substantial improvement of more than 20% across each evaluation metric, underscoring the significant value of the double fine-tuned technique in scenarios where the target dataset is limited. Additionally, the evaluation matrix maps indicate a more balanced distribution of true prediction samples compared to the single fine-tuned pre-trained model, demonstrating that the double fine-tuning technique can equally enhance the pre-trained model's robustness and reduce the risks of bias learning in multi-classification tasks.

Comparison with state-of-the-art Methods

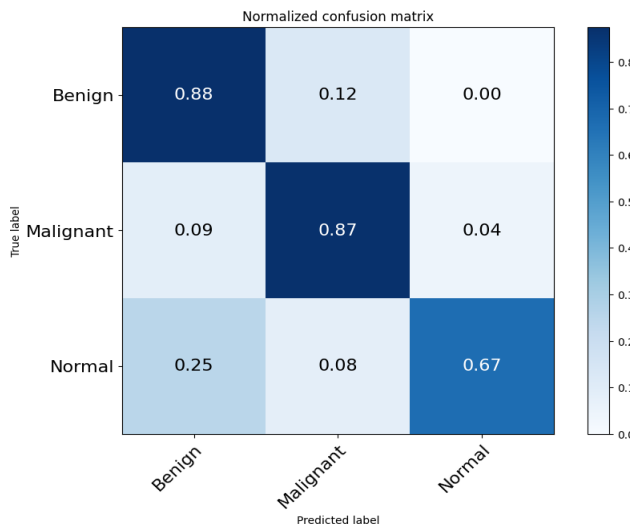
In this subsection, we conducted a comparative analysis, juxtaposing the optimal outcomes from both pre-trained methods against the performances of several contemporary state-of-the-art models. The objective is to elucidate the efficacy of the proposed pre-trained models on the selected datasets, and the results are delineated in Table 15. A discerning examination of the table reveals the superior performance of our proposed TL and SSL models compared to state-of-the-art models on four datasets. The proposed SSL model has achieved advantages of 4.8% and 5.2% in accuracy compared to those state-of-the-art DL models



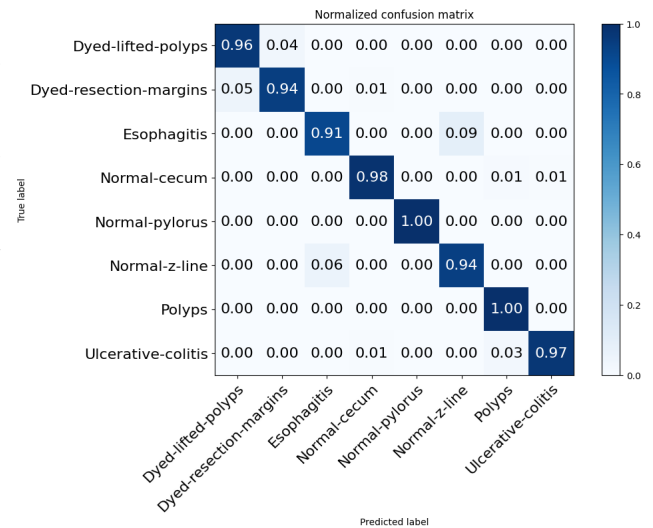
(a) Double fine-tuned SSL model on base BusI dataset



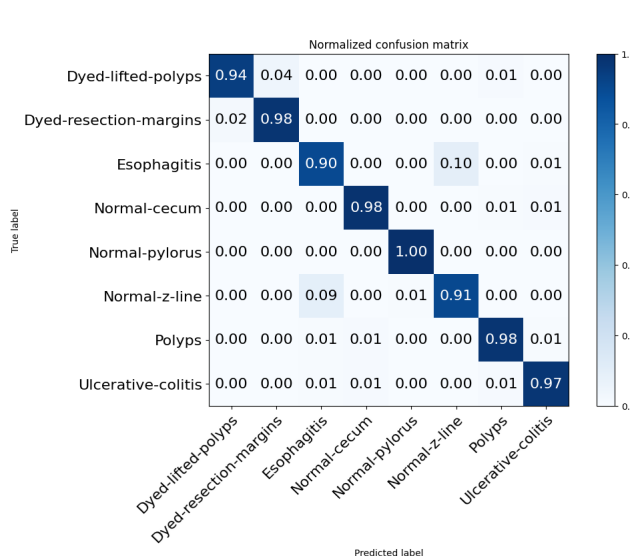
(b) Double fine-tuned SSL model on augmented BusI dataset



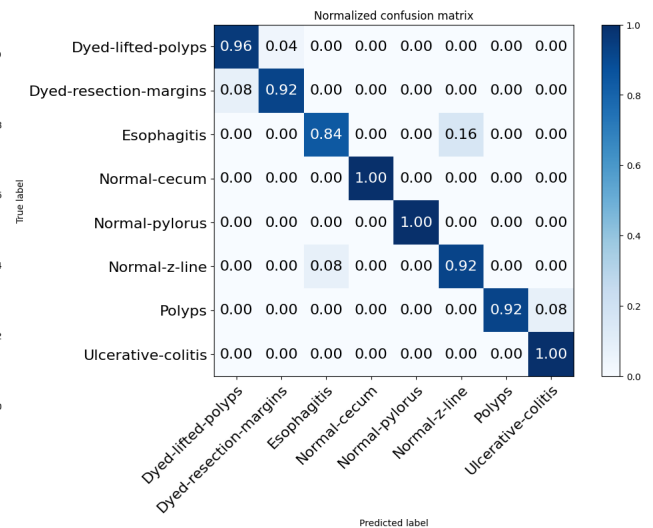
(c) Double fine-tuned SSL model on downsampled BusI dataset



(d) Double fine-tuned TL model on base KvasirV2 dataset



(e) Double fine-tuned TL model on augmented KvasirV2 dataset



(f) Double fine-tuned TL model on downsampled KvasirV2 dataset

Figure 11: Confusion matrix (a), (b), (c) represent double fine-tuned SSL model on BusI dataset, Confusion matrix (d), (e), (f) represent double fine-tuned TL model on KvasirV2 dataset.

Table 15

The proposed models versus state-of-the-art models.

Author	Models	Pretrained methods	Datasets	Acc(%)	Loss
Gheflati & Rivaz (2022)	ResNet-50	Transfer learning	BusI	83.00	-
Deb & Jha (2023)	Ensemble	Transfer learning	BusI	85.23	-
Proposed TL method	Xception	Transfer learning	BusI	77.50	1.18
Proposed SSL method	ResNet-50	Self-supervised learning	BusI	90.00	0.65
Dadgar & Neshat (2022)	InceptionResNetV2	Transfer learning	ChestCT	91.10	0.063
Mamun et al. (2023)	CNN	-	ChestCT	92.00	0.33
Proposed TL method	Xception	Transfer learning	ChestCT	93.30	0.26
Proposed SSL method	ResNet-50	Self-supervised learning	ChestCT	97.22	0.77
Dong et al. (2023)	Ensemble	Transfer learning	Kavisirv2	90.60	-
Mukhtorov et al. (2023)	ResNet-152	-	Kavisirv2	93.46	0.11
Wang et al. (2023)	Hybrid ViT	-	Kavisirv2	95.42	-
Proposed TL method	Xception	Transfer learning	Kavisirv2	96.40	0.40
Proposed SSL method	ResNet-50	Self-supervised learning	Kavisirv2	85.81	1.41
Kiefer et al. (2023)	MobileNetV3	Transfer Learning	EyePacs	88.30	-
Proposed TL method	Xception	Transfer learning	EyePacs	92.10	0.80
Proposed SSL method	ResNet-50	Self-supervised learning	EyePacs	83.20	0.48

that were either trained from scratch or employed transfer learning methodologies. This outcome aligns with the earlier experimental observation, indicating that the SSL method has more advantages in grey-scale medical image learning than the TL method. Concurrently, the proposed TL model demonstrated competitive prowess when compared to state-of-the-art DL models, showing a 1% improvement in the KvasirV2 dataset and a 4% improvement in the EyePacs dataset. This observation underscores the generalization ability and advanced performance of pre-trained TL models with ImageNet weight, showcasing that even the pre-trained ImageNet model is constrained in some scenarios but still has value in medical application learning.

Furthermore, by comparing with some DL studies trained from scratch, the TL model has shown additional advantages in training speed. For instance, Mukhtorov et al. (2023) reported that their CNN model, developed without the use of pre-training, necessitated a training duration of 6-12 hours from inception on the target Kvasirv2 dataset. In stark contrast, the pre-trained TL model required a mere 40 minutes for fine-tuning on the identical dataset, concurrently maintaining a better performance level during the testing phase. However, the pre-trained SSL model, on average, required double or triple the time compared to the TL model, consuming more time and computational resources in the training process. This high time consumption of SSL training has raised attention from researchers in achieving a balance between high model performance and reasonable time cost.

Comparison using XAI techniques

As emphasized in the literature review and recent studies (Albahri et al., 2023; Quinn et al., 2022), the reliability of AI applications in bio-medicine and healthcare has become a focal point of concern among researchers and medical institutions. This emphasis on trustworthiness holds pivotal significance for the widespread acceptance and integration

of AI within the medical domain. However, many studies have overlooked the importance of interpretability and robustness in their proposed models, potentially leaving researchers at risk when applying their work to real-world scenarios. In this section, we aim to test the robustness of our pre-trained models and demonstrate whether the proposed models have made reasonable predictions based on disease-type representations. To achieve this goal, we utilized Grad-CAM heatmaps to gain insights into the focus of the pre-trained models and to compare the predictions of the two pre-trained models. Understanding why one pre-trained model made correct predictions while the other did not is of significant value to the research. Specifically, we selected samples that were not classified into the true labels by one pre-trained model but were classified correctly by the other. We then employed the Grad-CAM technique to generate corresponding heatmaps and compared them to determine the reliability of correct predictions and identify areas for improvement in incorrect predictions.

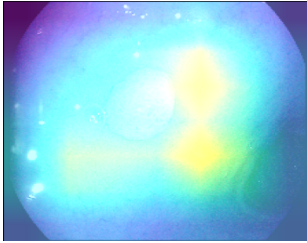
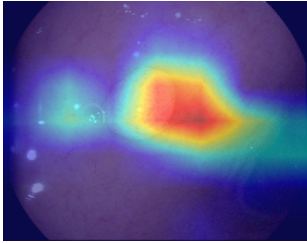
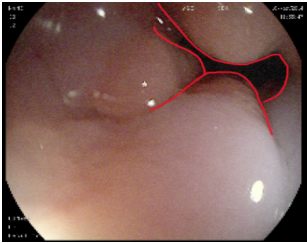
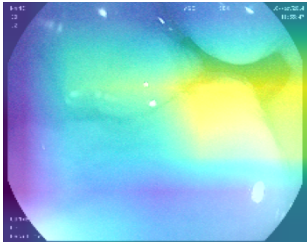
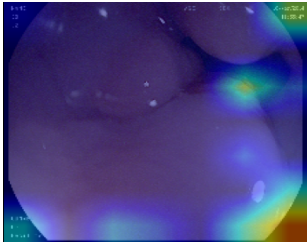
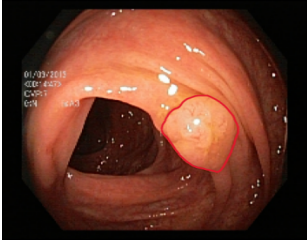
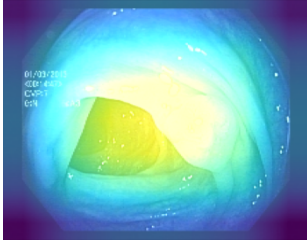
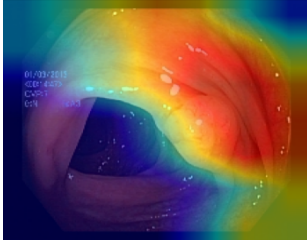
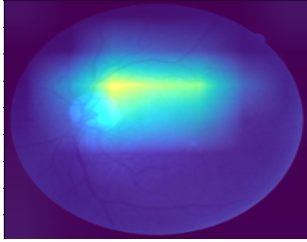
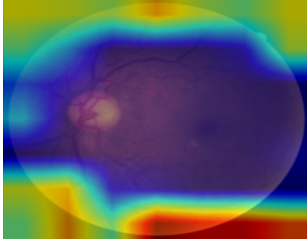
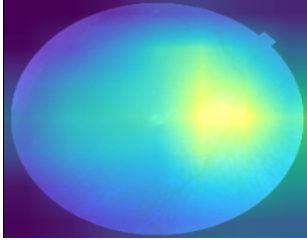
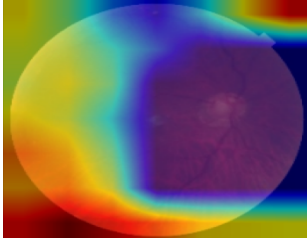
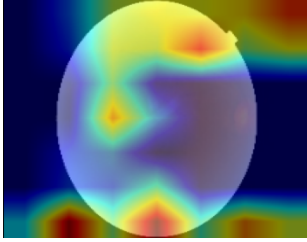
In Table 16, we conducted a comparative analysis of heatmaps generated from predicted samples sourced from grey-scale datasets including BusI and Chest CT. Each set includes the original sample with marked disease regions, followed by two heatmaps predicted by the pre-trained TL and SSL models, respectively. For the BusI dataset, we focused on samples from the Malignant class, as the primary objective of this dataset is to distinguish malignant tumours that pose a threat to patient health. The corresponding confusion matrices indicated that the pre-trained TL model struggled to classify this disease accurately. Malignant cancer typically presents with large tumour segments, shadows, and multiple projections from nodules. In the first BusI dataset sample, the TL model misclassified it as Benign, with its attention focused only on a fraction of the disease region, failing to encompass the entire area. In contrast, the SSL model correctly identified the disease region, indicating its ability to discern malignant tumours accurately. This trend persisted in the augmented BusI dataset, where the TL model

Table 16
The comparison of TL and SSL models' robustness towards grey-scale target datasets.

Datasets	Pretrained TL Model	Pretrained SSL Model	True Label
Bus1	Pred: Benign	Pred: Malignant	Malignant
Bus1 (Augmented)	Pred: Benign	Pred: Malignant	Malignant
Bus1 (Downsampled)	Pred: Benign	Pred: Malignant	Malignant
ChestCT	Pred: Adenocarcinoma	Pred: Squamous.Cell	Squamous.Cell
ChestCT (Augmented)	Pred: Adenocarcinoma	Pred: Large.Cell	Large.Cell
ChestCT (Downsampled)	Pred: Squamous.Cell	Pred: Large.Cell	Large.Cell

Table 17

The comparison of TL and SSL models' robustness towards colourful target datasets.

Datasets	Pretrained TL Model	Pretrained SSL Model	True Label
KvasirV2	Pred: Polyps	Pred: Ulcerative-colitis	Polyps
			
KvasirV2 (Augmented)	Pred: Normal-z-line	Pred: Normal-pylorus	Normal-z-line
			
KvasirV2 (Downsampled)	Pred: Ulcerative-colitis	Pred: Polyps	Polyps
			
EyePacs	Pred: RG	Pred: NRG	RG
			
EyePacs (Augmented)	Pred: RG	Pred: NRG	RG
			
EyePacs (Downsampled)	Pred: NRG	Pred: RG	NRG
			

again failed to fully capture the disease region, while the SSL model made the correct prediction. However, in the down-sampled BusI dataset, the SSL model, while correctly predicting the disease, lost focus on the true disease region, which highlights the potential negative impact of the down-sampling technique on model performance and robustness, particularly with limited target dataset sizes.

For the Chest CT dataset, samples were selected from the Squamous.cell.carcinoma and Large.cell.carcinoma classes, representing the main symptoms of lung cancer diseases. Squamous.cell.carcinoma typically exhibits cavitation and lung collapse, while Large.cell.carcinoma presents as large peripheral masses with irregular margins in lung segments. Accordingly, the pre-trained models should focus on the lung sides rather than soft tissues. In the Chest CT dataset, we isolated the lung sides from the original samples for comparison and heatmap evaluation. In the first image from the base ChestCT dataset, the TL model misclassified the disease as Adenocarcinoma, focusing its attention on the bottom segment of the right lung. In contrast, the SSL model correctly classified the sample, directing its attention to the right lung side and middle aorta and cavity, aligning more closely with the symptoms. In the second sample from the Large.cell.carcinoma class, the TL model improved its focus but still mispredicted the label, whereas the SSL model correctly classified the sample by widening its focus to both lung sides and middle tissue. In the down-sampled ChestCT sample, the TL model remained fixated on the right lung segment, focusing on white bubbles and nerves at the bottom, resulting in an incorrect prediction of Squamous.cell.carcinoma. In contrast, the SSL model correctly focused on the entire left lung segment and middle cavity, leading to an accurate prediction.

Table 17 presents a series of heat maps generated from colourful target datasets, specifically KvasirV2 and EyePacs. Within the KvasirV2 dataset, our analysis revealed challenges in classifying three pairs of classes: Dyed-lifted polyps versus Dyed-resection-margins; Esophagitis versus Normal z-line; Polyps versus Ulcerative-colitis. Among these pairs, Esophagitis and Polyps represent common esophageal diseases, prompting our focus on samples from the normal z-line and polyps to discern how TL and SSL models differentiate between them. The normal z-line typically features a clear demarcation at the oesophagus-stomach junction with uniform colour and smooth texture, similar to surrounding tissue. In contrast, Esophagitis often manifests as inflammation, erosion, or ulceration along the esophageal lining. Polyps exhibit discrete raised lesions with a smooth or lobulated surface, while Ulcerative Colitis presents diffuse inflammation, erythema, loss of vascular pattern, and friability in a continuous pattern. Taking advantage of these distinctions, we annotated the disease regions in the original images for comparative analysis. In the KvasirV2 dataset, the first Polyps sample shows substantial caking on the intestinal surface. The TL model correctly directed its attention around the caking, while the SSL model erroneously fixated on the caking itself, resulting in an incorrect prediction. In another

instance from the augmented KvasirV2 dataset, the TL model effectively discerned the demarcation between tissue and texture, accurately classifying the sample. Conversely, the SSL model misidentified the background, leading to an incorrect prediction of Normal-pylorus. In the downsampled KvasirV2 dataset, the attention of the TL model was dispersed between intestinal pores and caking tissue, resulting in misclassification. In contrast, the SSL model accurately identified Polyps by focusing on the caking tissue and part of the intestinal lining.

In the EyePacs dataset, the task revolves around distinguishing referable glaucoma (RG) and non-referable glaucoma (NRG) from colourful fundus images. Samples from both RG and NRG classes were examined. RG samples typically exhibit pronounced optic disc features such as cup-to-disc ratio, neuroretinal rim thinning, disc hemorrhages, and notching compared to NRG. The TL model effectively directed attention to the disc area, correctly classifying RG images. In contrast, the SSL model was fixated on the background of the image, leading to misclassifications. In an RG sample from the augmented EyePacs dataset, the TL model maintained accurate predictions by focussing on the disc area, while the SSL model failed to improve despite the augmentation, and fixated on the background. In the last sample with few optic disc features, the TL model correctly identified the white representation area, while the attention of the SSL model was divided between the eyecup and background, indicating a lack of true feature comprehension in NRG representations.

In summary, the heatmap samples generated through the Grad-CAM technique offer further evidence that both TL and SSL models not only exhibit distinct advantages in handling grey-scale and colourful medical images but also demonstrate superior robustness towards the specific image types in which they excel. These findings align closely with observations made during the training and testing phases, highlighting the efficacy of the pre-trained TL model in managing colourful medical images and the SSL model's remarkable capability in learning from grey-scale medical images.

5. Conclusion and Recommendation

In the realm of real-world medical diagnosis, advanced artificial intelligence techniques have assumed a pivotal role, with pre-trained methods that show significant potential in facilitating the integration of AI models into this domain. This study undertakes a comprehensive exploration of the strengths and limitations inherent in the two predominant pre-trained methods: transfer learning and self-supervised learning. The findings serve as a guiding resource for researchers, helping them select the most suitable pre-trained methods tailored to specific scenarios. The experimental analysis reveals that the TL method, coupled with widely employed ImageNet-pre-trained weights, excels in handling colourful medical datasets, but exhibits comparatively reduced efficacy in managing grey-scale medical datasets.

Conversely, the SSL method demonstrates superior performance when confronted with grey-scale medical datasets but lags behind the TL method in handling their colourful counterparts. Significantly, despite their shared objective of addressing data scarcity, models pre-trained using the SSL method exhibit heightened stability in the face of smaller datasets compared to those trained using the TL method. Additionally, the study examines the efficacy of data-altering methods in conjunction with pre-trained models for managing imbalanced data, which is an additional prevalent challenge in the medical field. The augmentation technique, when combined with pre-trained methods, not only enhances performance, but also fortifies the robustness of pre-trained models. Conversely, the down-sampling technique proves counterproductive, mitigating the influence of imbalanced class samples but compromising the overall performance and stability of the model.

A novel aspect of this study involves the evaluation of the double fine-tuning technique on both the pre-trained TL and SSL models. The observations affirm the utility of double fine-tuning in enhancing pre-trained models' performance and robustness, particularly in scenarios where it is hard to obtain extensive pre-trained data that matches the target data domain. The study introduced a modified Xception model and a concatenated ResNet-50 model, pre-trained using TL and SSL methods, respectively. The proposed SSL model achieves an accuracy of 90% and 97.22% in the multiclass classification of the augmented BusI and chest CT datasets. In contrast, the TL model achieves 96.4% and 92.1% accuracy in classifying the Kvasirv2 and EyePacs dataset image classes. These models, when fine-tuned with image-based AI technology, demonstrate efficacy in supporting disease diagnosis and classification.

The insights of this study have the potential to go beyond the realm of medical research, providing valuable considerations for addressing data scarcity through pre-trained methods in diverse fields. In addition, researchers who intend to utilise pre-trained techniques in their studies should consider the following conditions.

1. The SSL method is recommended for small target datasets (for example: less than 1000 samples), as it imparts superior performance and stability compared to the TL method.
2. The nature of the colour information within the target data samples dictates the choice between the TL and SSL methods. TL methods excel with colourful images, while SSL methods exhibit proficiency with grey-scale images.
3. When confronting imbalanced data, it is advisable to employ the data augmentation technique with pre-trained methods. However, researchers need to pay more attention to the associated increase in training time and computational resource consumption, as well as to the risk of overfitting.
4. Avoid using data down-sampling when the target dataset is small, as it may compromise model performance and robustness, leading to a loss of crucial target information.

5. In the absence of extensive source data that mirror target data features, consider a two-step approach: pre-training the model in a less related domain with more samples, followed by fine-tuning it in a closely related domain with smaller samples. This strategy bridges the gap between pre-trained models and target datasets without requiring abundant similar training samples.

6. Pre-trained methods extend their utility beyond small datasets; Even relatively large datasets benefit from improved performance, robustness, training speed, and avoidance of overfitting. Researchers are encouraged to explore pre-trained methods within and beyond the medical field.

CRediT authorship contribution statement

Zehui Zhao: Conceptualisation, Validation, Writing – original draft, **Laith Alzubaidi:** Conceptualisation, Resources, Formal analysis, Writing – review & editing, Validation, Supervision, **Jinglan Zhang:** Writing – review & editing, Formal analysis, Validation, Supervision **Ye Duan:** Formal analysis, Writing – review & editing, **Usman Naseem:** Formal analysis, Writing – review & editing, **Yuantong Gu:** Writing – review & editing, Validation, Funding acquisition.

Consent for publication

All authors have given their consent for publication.

Declaration of competing interest

All authors have declared that they have no conflict of interest.

Acknowledgements

I would like to thank my supervisors, colleagues, and reviewers for supporting my work and providing me with valuable feedback and suggestions.

Funding

Laith Alzubaidi and Yuantong Gu acknowledge the support received through the following funding schemes of the Australian Government: Australian Research Council (ARC) Industrial Transformation Training Centre (ITTC) for Joint Biomechanics under grant (IC190100020).

References

- Al-Dhabyani, W., Gomaa, M., Khaled, H., Fahmy, A., (2020). Dataset of breast ultrasound images. *Data in brief* 28, 104863. <https://doi.org/10.1016/j.dib.2019.104863>
- Albahri, A., Duhaim, A. M., Fadhel, M. A., Alnoor, A., Baqer, N. S., Alzubaidi, L., Albahri, O., Alamoody, A., Bai, J., Salhi, A., et al., (2023). A systematic review of trustworthy and explainable artificial intelligence in healthcare: Assessment of quality, bias risk, and data fusion. *Information Fusion*. <https://doi.org/10.1016/j.inffus.2023.03.008>
- Alzubaidi, L., Al-Amidie, M., Al-Asadi, A., Humaidi, A. J., Al-Shamma, O., Fadhel, M. A., Zhang, J., Santamaria, J., Duan, Y., (2021). Novel transfer learning approach for medical imaging with limited labeled data. *Cancers* 13 (7), 1590. <https://doi.org/10.3390/cancers13071590>

- Alzubaidi, L., Fadhel, M. A., Al-Shamma, O., Zhang, J., Santamaria, J., Duan, Y., R. Olewi, S., (2020). Towards a better understanding of transfer learning for medical imaging: a case study. *Applied Sciences* 10 (13), 4523. <https://doi.org/10.3390/app10134523>
- Anagha, C., Aishwarya, K., (2021). Pcos detection using ultrasound images. URL: <https://www.kaggle.com/datasets/anaghachoudhari/pcos-detection-using-ultrasound-images>
- Atasever, S., Azginoglu, N., Terzi, D. S., Terzi, R., (2023). A comprehensive survey of deep learning research on medical image analysis with focus on transfer learning. *Clinical Imaging* 94, 18–41. <https://doi.org/10.1016/j.clinimag.2022.11.003>
- Azizi, S., Culp, L., Freyberg, J., Mustafa, B., Baur, S., Kornblith, S., Chen, T., Tomasev, N., Mitrović, J., Strachan, P., et al., (2023). Robust and data-efficient generalization of self-supervised machine learning for diagnostic imaging. *Nature Biomedical Engineering*. <https://doi.org/10.1038/s41551-023-01049-7>
- Buda, M., Maki, A., Mazurowski, M. A., (2018). A systematic study of the class imbalance problem in convolutional neural networks. *Neural networks* 106, 249–259. <https://doi.org/10.1016/j.neunet.2018.07.011>
- Chen, T., Kornblith, S., Norouzi, M., Hinton, G., (2020). A simple framework for contrastive learning of visual representations. *International conference on machine learning*. PMLR, pp. 1597–1607.
- Chollet, F., (2017). Xception: Deep learning with depthwise separable convolutions. *Proceedings of the IEEE conference on computer vision and pattern recognition*. pp. 1251–1258.
- Combalia, M., Codella, N. C., Rotemberg, V., Helba, B., Vilaplana, V., Reiter, O., Carrera, C., Barreiro, A., Halpern, A. C., Puig, S., et al., (2019). Bcn20000: Dermoscopic lesions in the wild. *arXiv preprint arXiv:1908.02288*. <https://doi.org/10.48550/arXiv.1908.02288>
- Dadgar, S., Neshat, M., (2022). Comparative hybrid deep convolutional learning framework with transfer learning for diagnosis of lung cancer. *International Conference on Soft Computing and Pattern Recognition*. Springer, pp. 296–305.
- Deb, S. D., Jha, R. K., (2023). Breast ultrasound image classification using fuzzy-rank-based ensemble network. *Biomedical Signal Processing and Control* 85, 104871. <https://doi.org/10.1016/j.bspc.2023.104871>
- Del Pup, F., Atzori, M., (2023). Applications of self-supervised learning to biomedical signals: a survey. *IEEE Access*. <https://doi.org/10.1109/ACCESS.2023.3344531>
- Dong, Z., Xu, B., Shi, J., Zheng, L., (2023). Local and global feature interaction network for endoscope image classification. *International Conference on Image and Graphics*. Springer, pp. 412–424.
- Ericsson, L., Gouk, H., Hospedales, T. M., (2021). How well do self-supervised models transfer? *Proceedings of the IEEE/CVF Conference on Computer Vision and Pattern Recognition*. pp. 5414–5423.
- Ericsson, L., Gouk, H., Hospedales, T. M., (2022a). Why do self-supervised models transfer? on the impact of invariance on downstream tasks. *33rd British Machine Vision Conference 2022, BMVC 2022, London, UK, November 21-24*. BMVA Press, p. 14.
- Ericsson, L., Gouk, H., Loy, C. C., Hospedales, T. M., (2022b). Self-supervised representation learning: Introduction, advances, and challenges. *IEEE Signal Processing Magazine* 39 (3), 42–62. <https://doi.org/10.1109/MSP.2021.3134634>
- Gheflati, B., Rivaz, H., (2022). Vision transformers for classification of breast ultrasound images. *2022 44th Annual International Conference of the IEEE Engineering in Medicine & Biology Society (EMBC)*. IEEE, pp. 480–483. <https://doi.org/10.1109/EMBC48229.2022.9871809>
- Haixiang, G., Yijing, L., Shang, J., Mingyun, G., Yuanyue, H., Bing, G., (2017). Learning from class-imbalanced data: Review of methods and applications. *Expert systems with applications* 73, 220–239. <https://doi.org/10.1016/j.eswa.2016.12.035>
- Hany, M., (2020). Chest ct-scan images dataset. URL: <https://www.kaggle.com/datasets/mohamedhanyyy/chest-ctscan-images>
- He, K., Zhang, X., Ren, S., Sun, J., (2016). Deep residual learning for image recognition. *Proceedings of the IEEE conference on computer vision and pattern recognition*. pp. 770–778.
- Hosseinzadeh Taher, M. R., Haghghi, F., Feng, R., Gotway, M. B., Liang, J., (2021). A systematic benchmarking analysis of transfer learning for medical image analysis. *Domain Adaptation and Representation Transfer, and Affordable Healthcare and AI for Resource Diverse Global Health: Third MICCAI Workshop, DART 2021, and First MICCAI Workshop, FAIR 2021, Held in Conjunction with MICCAI 2021, Strasbourg, France, September 27 and October 1, 2021, Proceedings 3*. Springer, pp. 3–13.
- Huh, M., Agrawal, P., Efron, A. A., (2016). What makes imagenet good for transfer learning? *arXiv preprint arXiv:1608.08614*. <https://doi.org/10.48550/arXiv.1608.08614>
- Islam, M. N., Hasan, M., Hossain, M. K., Alam, M. G. R., Uddin, M. Z., Soylu, A., (2022). Vision transformer and explainable transfer learning models for auto detection of kidney cyst, stone and tumor from ct-radiography. *Scientific Reports* 12 (1), 11440. <https://doi.org/10.1038/s41598-022-15634-4>
- Kassani, S. H., Kassani, P. H., Khazaeinezhad, R., Wesolowski, M. J., Schneider, K. A., Deters, R., (2019). Diabetic retinopathy classification using a modified xception architecture. *2019 IEEE international symposium on signal processing and information technology (ISSPIT)*. IEEE, pp. 1–6. <https://doi.org/10.1109/ISSPIT47144.2019.9001846>
- Kiefer, R., Abid, M., Ardali, M. R., Steen, J., Amjadian, E., (2023). Automated fundus image standardization using a dynamic global foreground threshold algorithm. *2023 8th International Conference on Image, Vision and Computing (ICIVC)*. IEEE, pp. 460–465. <https://doi.org/10.1109/ICIVC58118.2023.10270429>
- Kim, H. E., Cosa-Linan, A., Santhanam, N., Jannesari, M., Maros, M. E., Ganslandt, T., (2022). Transfer learning for medical image classification: a literature review. *BMC medical imaging* 22 (1), 69. <https://doi.org/10.1186/s12880-022-00793-7>
- Kolesnikov, A., Beyer, L., Zhai, X., Puigcerver, J., Yung, J., Gelly, S., Houlsby, N., (2020). Big transfer (bit): General visual representation learning. *Computer Vision—ECCV 2020: 16th European Conference, Glasgow, UK, August 23–28, 2020, Proceedings, Part V 16*. Springer, pp. 491–507.
- Kornblith, S., Shlens, J., Le, Q. V., (2019). Do better imagenet models transfer better? *Proceedings of the IEEE/CVF conference on computer vision and pattern recognition*. pp. 2661–2671.
- Krishnan, R., Rajpurkar, P., Topol, E. J., (2022). Self-supervised learning in medicine and healthcare. *Nature Biomedical Engineering* 6 (12), 1346–1352. <https://doi.org/10.1038/s41551-022-00914-1>
- Krizhevsky, A., Sutskever, I., Hinton, G. E., (2012). Imagenet classification with deep convolutional neural networks. *Advances in neural information processing systems* 25.
- Liu, Y., Zhang, L., Hao, Z., Yang, Z., Wang, S., Zhou, X., Chang, Q., (2022). An xception model based on residual attention mechanism for the classification of benign and malignant gastric ulcers. *Scientific Reports* 12 (1), 15365. <https://doi.org/10.1038/s41598-022-19639-x>
- Mamun, M., Mahmud, M. I., Meherin, M., Abdelgawad, A., (2023). Lcdctcnn: Lung cancer diagnosis of ct scan images using cnn based model. *2023 10th International Conference on Signal Processing and Integrated Networks (SPIN)*. IEEE, pp. 205–212. <https://doi.org/10.1109/SPIN57001.2023.10116075>
- Marcus, D. S., Wang, T. H., Parker, J., Csernansky, J. G., Morris, J. C., Buckner, R. L., (2007). Open access series of imaging studies (oasis): cross-sectional mri data in young, middle aged, nondemented, and demented older adults. *Journal of cognitive neuroscience* 19 (9), 1498–1507. <https://doi.org/10.1162/jocn.2007.19.9.1498>
- Morid, M. A., Borjali, A., Del Fiol, G., (2021). A scoping review of transfer learning research on medical image analysis using imagenet. *Computers in biology and medicine* 128, 104115. <https://doi.org/10.1016/j.combiomed.2020.104115>
- Mukhtorov, D., Rakhmonova, M., Muksimova, S., Cho, Y.-I., (2023). Endoscopic image classification based on explainable deep learning. *Sensors* 23 (6), 3176. <https://doi.org/10.3390/s23063176>
- Muljo, H. H., Pardamean, B., Elwirehardja, G. N., Hidayat, A. A., Sudigyo, D., Rahutomo, R., Cenggoro, T. W., (2023). Handling severe data imbalance in chest x-ray image classification with transfer learning using swav self-supervised pre-training. *Commun. Math. Biol. Neurosci.* 2023, Article-ID.

- Neyshabur, B., Sedghi, H., Zhang, C., (2020). What is being transferred in transfer learning? *Advances in neural information processing systems* 33, 512–523.
- Nguyen, H. Q., Lam, K., Le, L. T., Pham, H. H., Tran, D. Q., Nguyen, D. B., Le, D. D., Pham, C. M., Tong, H. T., Dinh, D. H., et al., (2022). Vindr-cxr: An open dataset of chest x-rays with radiologist's annotations. *Scientific Data* 9 (1), 429. <https://doi.org/10.1038/s41597-022-01498-w>
- Niu, S., Liu, Y., Wang, J., Song, H., (2020). A decade survey of transfer learning (2010–2020). *IEEE Transactions on Artificial Intelligence* 1 (2), 151–166. <https://doi.org/10.1109/TAI.2021.3054609>
- Pan, S. J., Yang, Q., (2010). A survey on transfer learning. *IEEE Transactions on knowledge and data engineering* 22 (10), 1345–1359. <https://doi.org/10.1109/TKDE.2009.191>
- Patil, R., Sharma, S., (2024). Automatic glaucoma detection from fundus images using transfer learning. *Multimedia Tools and Applications*, 1–20. <https://doi.org/10.1007/s11042-024-18242-8>
- Pogorelov, K., Randel, K. R., Griwodz, C., Eskeland, S. L., de Lange, T., Johansen, D., Spampinato, C., Dang-Nguyen, D.-T., Lux, M., Schmidt, P. T., et al., (2017). Kvasir: A multi-class image dataset for computer aided gastrointestinal disease detection. *Proceedings of the 8th ACM on Multimedia Systems Conference*. pp. 164–169. <https://doi.org/10.1145/3083187.3083212>
- Pogorelov, K., Riegler, M., Halvorsen, P., Hicks, S., Randel, K. R., Dang Nguyen, D. T., Lux, M., Ostroukhova, O., de Lange, T., (2018). Medico multimedia task at mediaeval 2018. *CEUR Workshop Proceedings*. Vol. 2283. Technical University of Aachen, pp. 1–4.
- Qayyum, A., Qadir, J., Bilal, M., Al-Fuqaha, A., (2020). Secure and robust machine learning for healthcare: A survey. *IEEE Reviews in Biomedical Engineering* 14, 156–180. <https://doi.org/10.1109/RBME.2020.3013489>
- Quinn, T. P., Jacobs, S., Senadeera, M., Le, V., Coghlan, S., (2022). The three ghosts of medical ai: Can the black-box present deliver? *Artificial intelligence in medicine* 124, 102158. <https://doi.org/10.1016/j.artmed.2021.102158>
- Raghu, M., Zhang, C., Kleinberg, J., Bengio, S., (2019). Transfusion: Understanding transfer learning for medical imaging. *Advances in neural information processing systems* 32.
- Razzak, M. I., Naz, S., Zaib, A., (2018). Deep learning for medical image processing: Overview, challenges and the future. *Classification in BioApps: Automation of Decision Making*, 323–350.
- Romero, M., Interian, Y., Solberg, T., Valdes, G., (2020). Targeted transfer learning to improve performance in small medical physics datasets. *Medical physics* 47 (12), 6246–6256. <https://doi.org/10.1002/mp.14507>
- Russakovsky, O., Deng, J., Su, H., Krause, J., Satheesh, S., Ma, S., Huang, Z., Karpathy, A., Khosla, A., Bernstein, M., et al., (2015). Imagenet large scale visual recognition challenge. *International journal of computer vision* 115, 211–252. <https://doi.org/10.1007/s11263-015-0816-y>
- Schiappa, M. C., Rawat, Y. S., Shah, M., (2023). Self-supervised learning for videos: A survey. *ACM Computing Surveys* 55 (13s), 1–37. <https://doi.org/10.1145/3577925>
- Selvaraju, R. R., Cogswell, M., Das, A., Vedantam, R., Parikh, D., Batra, D., (2017). Grad-cam: Visual explanations from deep networks via gradient-based localization. *Proceedings of the IEEE international conference on computer vision*. pp. 618–626.
- Shorten, C., Khoshgoftaar, T. M., (2019). A survey on image data augmentation for deep learning. *Journal of big data* 6 (1), 1–48. <https://doi.org/10.1186/s40537-019-0197-0>
- Shurrab, S., Duwairi, R., (2022). Self-supervised learning methods and applications in medical imaging analysis: A survey. *PeerJ Computer Science* 8, e1045. <https://doi.org/10.7717/peerj-cs.1045>
- Tan, Z., Yu, Y., Meng, J., Liu, S., Li, W., (2024). Self-supervised learning with self-distillation on covid-19 medical image classification. *Computer Methods and Programs in Biomedicine* 243, 107876. <https://doi.org/10.1016/j.cmpb.2023.107876>
- Truong, T., Mohammadi, S., Lenga, M., (2021). How transferable are self-supervised features in medical image classification tasks? *Machine Learning for Health*. PMLR, pp. 54–74.
- Wang, K., (2021). An overview of deep learning based small sample medical imaging classification. *2021 International Conference on Signal Processing and Machine Learning (CONF-SPML)*. IEEE, pp. 278–281. <https://doi.org/10.1109/CONF-SPML54095.2021.00060>
- Wang, W., Yang, X., Tang, J., (2023). Vision transformer with hybrid shifted windows for gastrointestinal endoscopy image classification. *IEEE Transactions on Circuits and Systems for Video Technology*. <https://doi.org/10.1109/TCSVT.2023.3277462>
- Wu, R., Liang, C., Li, Y., Shi, X., Zhang, J., Huang, H., (2023). Self-supervised transfer learning framework driven by visual attention for benign–malignant lung nodule classification on chest ct. *Expert Systems with Applications* 215, 119339. <https://doi.org/10.1016/j.eswa.2022.119339>
- Yang, X., He, X., Liang, Y., Yang, Y., Zhang, S., Xie, P., (2020). Transfer learning or self-supervised learning? a tale of two pretraining paradigms. *arXiv preprint arXiv:2007.04234*. <https://doi.org/10.48550/arXiv.2007.04234>
- Zhang, C., Zheng, H., Gu, Y., (2023). Dive into the details of self-supervised learning for medical image analysis. *Medical Image Analysis* 89, 102879. <https://doi.org/10.1016/j.media.2023.102879>
- Zhang, W., Deng, L., Zhang, L., Wu, D., (2022). A survey on negative transfer. *IEEE/CAA Journal of Automatica Sinica* 10 (2), 305–329. <https://doi.org/10.1109/JAS.2022.106004>
- Zhao, Z., Alzubaidi, L., Zhang, J., Duan, Y., Gu, Y., (2023). A comparison review of transfer learning and self-supervised learning: Definitions, applications, advantages and limitations. *Expert Systems with Applications*, 122807. <https://doi.org/10.1016/j.eswa.2023.122807>
- Zhou, B., Khosla, A., Lapedriza, A., Oliva, A., Torralba, A., (2016). Learning deep features for discriminative localization. *Proceedings of the IEEE conference on computer vision and pattern recognition*. pp. 2921–2929.